



HAL
open science

Influence of anthropogenic emission inventories on simulations of air quality in China during winter and summer 2010

Idir Bouarar, Guy Brasseur, Katinka Petersen, Claire Granier, Lili Wang, Ying Xie, Qi Fan, Xuemei Wang, Dongsheng Ji, Zirui Liu, et al.

► **To cite this version:**

Idir Bouarar, Guy Brasseur, Katinka Petersen, Claire Granier, Lili Wang, et al.. Influence of anthropogenic emission inventories on simulations of air quality in China during winter and summer 2010. Atmospheric Environment, 2019, 198, pp.236-256. 10.1016/j.atmosenv.2018.10.043 . hal-02116043

HAL Id: hal-02116043

<https://hal.science/hal-02116043>

Submitted on 10 Nov 2020

HAL is a multi-disciplinary open access archive for the deposit and dissemination of scientific research documents, whether they are published or not. The documents may come from teaching and research institutions in France or abroad, or from public or private research centers.

L'archive ouverte pluridisciplinaire **HAL**, est destinée au dépôt et à la diffusion de documents scientifiques de niveau recherche, publiés ou non, émanant des établissements d'enseignement et de recherche français ou étrangers, des laboratoires publics ou privés.

Manuscript Number: ATMENV-D-18-00596

Title: Modelling trace gas and aerosol distribution in China during winter and summer 2010

Article Type: Research Paper

Keywords: Air quality modelling; WRF-Chem; PM2.5; Ozone; Anthropogenic Emissions

Corresponding Author: Dr. Idir Bouarar,

Corresponding Author's Institution: Max Planck Institute for Meteorology

First Author: Idir Bouarar

Order of Authors: Idir Bouarar; Guy Brasseur; Katinka Petersen; Claire Granier; Lili Wang; Ying Xie; Fan Qi; Xuemei Wang; Dongsheng Ji; Zirui Liu; Wei Gao

Abstract: We applied the regional chemistry-transport model WRF-Chem to investigate the air pollution characteristics in three Chinese city clusters (Beijing, Shanghai and Guangzhou) and assess the model performance in wintertime (January 2010) and summertime (July 2010) conditions. Three simulations utilizing the HTAPv2, REASv2 and MACCity anthropogenic emission inventories were conducted and compared with satellite and ground-based measurements to assess the sensitivity of the model predictions to anthropogenic emissions. Model-predicted surface meteorological fields are overall in good agreement with surface observations, although the model tends to overestimate the maximum values of surface wind speed as reported also in previous WRF-Chem modelling studies. Large discrepancies between the three emission inventories were found, specifically in the spatial distribution and the magnitude of the emissions (e.g. over 98%, 86% and 85% differences in some regions for carbon monoxide (CO), nitrogen oxide (NO) and organic carbon (OC) emissions respectively). As a result, we found large differences between the simulations and several discrepancies when compared to satellite and surface observations. The HTAPv2- and REASv2-based simulations better reproduce the magnitude and spatial features of CO total columns and NO₂ tropospheric columns derived from MOPITTv6 and GOME2 satellite observations respectively. The three model simulations satisfactorily reproduce the air pollution characteristics in January 2010 as observed at surface monitoring stations in Beijing and Shanghai, and meet the air quality model performance goals for particulates. The HTAPv2-based simulation better captures the pollution episode that occurred in Beijing in mid-January 2010, which is found to be related to a combination of different meteorological factors that led to the build-up of pollution. The high photochemical activity and convective turbulence in July 2010, in addition to differences in the emissions used, led to more pronounced differences between the three simulations and lower statistical skills in particular for trace gases. This study shows that a considerable part of uncertainties in current air quality model predictions for China can be attributed to uncertainties in

emissions estimates in the anthropogenic emission inventories. It highlights the need for more accurate and highly resolved emissions in order to improve the accuracy of the model predictions. This study reveals however that in some cases, model-observation discrepancies cannot be attributed only to inaccuracies in the emissions. For example, we found that regardless of the adopted emissions, all the simulations failed to capture the variability of particulate matter in Guangzhou in January 2010 indicating that other factors than emissions have a considerable influence on the atmospheric composition in this region. This work shows that inaccuracies in the predicted meteorological parameters (e.g. wind speed/direction, relative humidity, etc.) can significantly affect the model performance as found for example in the model predictions for Shanghai for July 2010, which showed high and abrupt increases of NO_x and particulates due to rapid decreases in wind speed in the model.

April 10th, 2018

Dear Editor,

I, as corresponding author on behalf of all the authors, am submitting a manuscript entitled: Modelling trace gas and aerosol distribution in China during winter and summer 2010. Please accept the manuscript for consideration to be published in the journal Atmospheric Environment.

The manuscript, which is in the scope of Atmospheric Environment, is a research paper to investigate the air pollution characteristics in three polluted cities in China (Beijing, Shanghai and Guangzhou) in winter and summer conditions using the regional WRF-Chem model simulations combined with ground-based and satellite measurements. The ability of WRF-Chem to reproduce the distributions and concentrations of pollutants in Eastern China and to capture specific pollution events under specific meteorological conditions is assessed. The study shows the uncertainties in current air quality model predictions for China related to uncertainties in estimates of anthropogenic emissions in the current inventories. It highlights the need for more accurate and highly resolved emissions in order to improve the accuracy of the model predictions. The study demonstrates also the considerable impact of inaccuracies in the prediction of meteorological situations on the performance and statistical skills of the air quality predictions. The study provided also an opportunity to assess the performance of the selected WRF-Chem model settings, which led to the implementation of the model as an operational forecasting system for regional air quality in China.

We affirm that this manuscript is original, has not been published before and is not currently being considered for publication elsewhere.

Sincerely yours,

Idir Bouarar
Max Planck Institute for Meteorology
Environmental Modeling
Bundesstr. 53
D-20146 Hamburg
Germany

E-mail: idir.bouarar@mpimet.mpg.de
Tel.: +49-(0)40-41173-411

1 **Modelling trace gas and aerosol distribution in China during winter** 2 **and summer 2010**

3 Idir Bouarar¹, Guy Brasseur¹, Katinka Petersen¹, Claire Granier^{2,3}, Qi Fan⁴, Xuemei Wang⁵, Lili Wang⁶,
4 Dongsheng Ji⁶, Zirui Liu⁶, Ying Xie⁷, Wei Gao⁷

5 ¹Max Planck Institute for Meteorology, Hamburg, Germany

6 ²Laboratoire d'Aérodologie, CNRS-UPS, Toulouse, France

7 ³NOAA ESRL/CSD and CIRES, University Colorado, Boulder, USA

8 ⁴Sun Yat-Sen University, School Of Environmental Science and Engineering (SESE-SYSU), Guangzhou, China

9 ⁵Institute for Environmental and Climate Research, Jinan University, Guangzhou, China

10 ⁶State Key Laboratory of Atmospheric Boundary Layer Physics and Atmospheric Chemistry, Institute of Atmospheric Physi
11 cs, Chinese Academy of Sciences, Beijing, China

12 ⁷Yangtze River Delta Center for Environmental Meteorology Prediction and Warning, Shanghai Meteorological
13 Service, Shanghai, China

14

15 *Correspondence to:* Idir Bouarar (idir.bouarar@mpimet.mpg.de)

16 **Abstract**

17 We applied the regional chemistry-transport model WRF-Chem to investigate the air pollution
18 characteristics in three Chinese city clusters (Beijing, Shanghai and Guangzhou) and assess the model
19 performance in wintertime (January 2010) and summertime (July 2010) conditions. Three simulations
20 utilizing the HTAPv2, REASv2 and MACCity anthropogenic emission inventories were conducted and
21 compared with satellite and ground-based measurements to assess the sensitivity of the model
22 predictions to anthropogenic emissions. Model-predicted surface meteorological fields are overall in
23 good agreement with surface observations, although the model tends to overestimate the maximum
24 values of surface wind speed as reported also in previous WRF-Chem modelling studies. Large
25 discrepancies between the three emission inventories were found, specifically in the spatial distribution
26 and the magnitude of the emissions (e.g. over 98%, 86% and 85% differences in some regions for
27 carbon monoxide (CO), nitrogen oxide (NO) and organic carbon (OC) emissions respectively). As a
28 result, we found large differences between the simulations and several discrepancies when compared to
29 satellite and surface observations. The HTAPv2- and REASv2-based simulations better reproduce the
30 magnitude and spatial features of CO total columns and NO₂ tropospheric columns derived from

31 MOPITTv6 and GOME2 satellite observations respectively. The three model simulations satisfactorily
32 reproduce the air pollution characteristics in January 2010 as observed at surface monitoring stations in
33 Beijing and Shanghai, and meet the air quality model performance goals for particulates. The HTAPv2-
34 based simulation better captures the pollution episode that occurred in Beijing in mid-January 2010,
35 which is found to be related to a combination of different meteorological factors that led to the build-up
36 of pollution. The high photochemical activity and convective turbulence in July 2010, in addition to
37 differences in the emissions used, led to more pronounced differences between the three simulations and
38 lower statistical skills in particular for trace gases.

39 This study shows that a considerable part of uncertainties in current air quality model predictions for
40 China can be attributed to uncertainties in emissions estimates in the anthropogenic emission
41 inventories. It highlights the need for more accurate and highly resolved emissions in order to improve
42 the accuracy of the model predictions. This study reveals however that in some cases, model-
43 observation discrepancies cannot be attributed only to inaccuracies in the emissions. For example, we
44 found that regardless of the adopted emissions, all the simulations failed to capture the temporal
45 variability of particulate matter in Guangzhou in January 2010 indicating that other factors than
46 emissions have a considerable influence on the atmospheric composition in this region. This work
47 shows that inaccuracies in the predicted meteorological parameters (e.g. wind speed/direction, relative
48 humidity, etc.) can significantly affect the model performance as found for example in the model
49 predictions for Shanghai for July 2010, which showed high and abrupt increases of NO_x and
50 particulates due to rapid decreases in wind speed in the model.

51

52 **Keywords:** Air quality modelling; WRF-Chem; PM_{2.5}; Ozone; Anthropogenic Emissions

53

54 **1. Introduction**

55 Air pollutants such as ozone (O₃), nitrogen oxides (NO_x), carbon monoxide (CO), sulfur dioxide (SO₂)
56 and particulate matter (PM_{2.5} and PM₁₀) are known to have severe and acute effects on human health.
57 Several studies have shown a wide range of these effects extending from minor respiratory infections
58 and bronchitis to chronic effects, heart and vascular diseases and even lung cancer (Kampa and
59 Castanas 2008; Hamra et al. 2015). Air pollutants are known to have also adverse consequences on
60 agriculture by reducing productivity and crop yields in response to acid precipitation and dry deposition

61 of ozone and other pollutants (Ashmore, 2005; Leisner et al., 2012; Sinha et al., 2015). Other adverse
62 effects include reduction in visibility, forest damage, eutrophication of water resources, and damages to
63 buildings and historical monuments. Air pollutants contribute also to global warming due to direct and
64 indirect radiative forcing (Sitch et al. 2007), thus affecting climate change (Brasseur et al., 1999;
65 Akimoto, 2003).

66 China has been experiencing rapid industrialization for more than three decades. During the course of
67 this expansion, urbanization and consequently energy needs increased, causing significant impacts on
68 the environment including air and water quality degradation. Among the environmental issues in China,
69 air quality has become a major problem and several studies and efforts have been devoted to elucidate
70 the reasons behind the extremely high pollution events that occur frequently in China. Bouarar et al.
71 (2017) presented an integrated view of past and present situations in China and a comprehensive
72 analysis of the chemical and meteorological processes responsible for the formation of air pollutants in
73 eastern Asia. Guo et al. (2014) showed that, although observed chemical compositions of particles in
74 Beijing are similar to those observed in other regions of the world, this city and likely other urban areas
75 in China are characterised by particular aerosol formation mechanisms leading to high PM_{2.5}. Based on
76 in-situ observations, Huang et al. (2014) analysed the chemical nature and source of PM_{2.5} in urban
77 locations in China during the extremely severe haze pollution in January 2013, and found that
78 secondary aerosol formation was the main contribution to this haze pollution event. Wang et al. (2014)
79 concluded that secondary aerosol formation is an important mechanism in the development of heavy
80 haze episodes. Specific meteorological conditions together with specific geographical characteristics
81 can lead to air stagnation and low mixing in the boundary layer, which reduce the dispersion of
82 pollution and thus lead to pollution accumulation near the surface (Wang et al., 2014; Zhao et al., 2013;
83 Bouarar et al., 2017).

84 Air quality issues in China have also become a major concern for many other countries that are directly
85 affected through long-range transport of pollution. The close countries such as Japan and Korea are the
86 first affected by pollution transported downwind from eastern China (Kurokawa et al., 2009; Osada et
87 al., 2009; Chatani and Sudo, 2011; Geng et al., 2014). Several studies on transport pathways of
88 pollution have demonstrated the transpacific transport of East Asian emissions and their potential
89 contribution to pollution episodes in western USA (Jacob et al, 1999; Liang et al. 2004; Zhang et al.,
90 2009; Lin et al., 2012). Stohl et al. (2007) showed that air pollution plumes from Southeast Asia can

91 also reach the upper troposphere in Europe. Detailed pathways of pollutants export originating in east
92 Asia are identified and analysed in UNECE (2010), showing that air pollution in Asia affects other
93 regions of the world.

94 Air quality models, with their ability to simulate the physical and chemical processes that affect air
95 pollution, are powerful tools used together with observational datasets to address the complex chemical
96 processes and source and dispersion of pollution within the atmosphere (Brasseur and Jacob, 2017).
97 They are also important tools for air quality management and policy assessments, and can assist for
98 defining effective strategies and plans to mitigate air pollution. Mesoscale models have been
99 increasingly used to investigate air pollution characteristics in many countries especially in Asia. Xu et
100 al. (2008) analysed the chemical regimes responsible for summertime O₃ formation in the Beijing area
101 using an air quality model. Liao et al. (2014), showed a clear sensitivity of regional simulation of O₃,
102 particles and meteorological variables in the Yangtze River Delta region to urban canopy
103 parameterisations. Fan et al. (2015) analysed three pollution episodes in the Pearl River Delta region
104 based on air quality model simulations, and demonstrated the impact of local emissions and the role of
105 weather conditions, such as high humidity and cloud processes, in the formation of fine secondary
106 particles. Wang et al. (2010) showed that seasonal, day-of-week, diurnal and vertical allocations of
107 anthropogenic emissions can significantly change the simulated distribution of NO_x, SO₂ and O₃
108 concentrations in a mesoscale model. From the analysis of their global and regional model results,
109 Quennehen et al. (2016) investigated the distribution of pollutants in summer 2008 and showed that,
110 despite some similarities (e.g. overestimation of surface NO₂), the accuracy of simulated O₃ and aerosol
111 patterns often vary considerably among the models.

112 Despite several modelling studies that have focused on air pollution events in China, the complex
113 formation mechanisms of acute events still need to be elucidated, and the state-of-the-art chemical
114 transport models are still unable to predict correctly the magnitude and characteristics of such pollution
115 episodes. Model treatments of processes affecting the lifetime, formation and dispersion of pollutants
116 still need to be improved (Quennehen et al., 2016; Bouarar et al., 2017). Other uncertainties in air
117 quality model predictions are related to model input datasets including initial and boundary conditions,
118 meteorological data and surface emission fluxes. For the latter, there are numerous inventories
119 providing estimates of surface emissions at both the global and regional scales. However, several
120 assessments of the quality of such datasets exhibit large differences not only in the estimated total

121 amounts (Kurokawa et al., 2013) but also in the spatial and temporal distributions of past, present and
122 future emissions (Granier et al. 2011). Differences in estimates of activity data and emissions factors for
123 different sources and sectors are among the possible reasons of discrepancies between the inventories
124 (Granier et al., 2017).

125 Previous modelling studies either focused on a specific region of Asia, a specific pollution event and
126 period, or analysed observations and model results only for some specific chemical species. Moreover,
127 only few studies have been dedicated to the impact of uncertainties in emissions inventories on air
128 quality model results particularly in Asia (e.g. Amnuaylojaroen et al., 2014). In the present study, we
129 investigate the distribution of air pollutants in three major urban areas: Beijing, Shanghai and
130 Guangzhou. These regions have experienced intense urbanization and population growth during the last
131 decades and are among the most polluted areas of China (Wu et al., 2012; Boynard et al., 2014). We
132 investigate specifically the sensitivity of WRF-Chem air quality predictions to uncertainties in
133 emissions using three anthropogenic emission inventories. The HTAPv2 inventory (developed within
134 the Task Force Hemispheric Transport of Air Pollution initiative TF HTAP) is being used in many
135 modelling activities including the WRF-Chem operational air quality forecasting system that we
136 implemented within the framework of the EU FP7 project PANDA (www.marcopolo-panda.eu). The
137 MACCity inventory (developed within the MACC and CityZen EU projects) is currently used by the
138 Copernicus Atmospheric Monitoring Service (CAMS) (Flemming et al., 2009, 2017). REASv2
139 (Regional Emission Inventory in Asia version 2) is among the first inventories that provided emissions
140 at high spatial resolution for several East Asian countries. We analyse the model results and the
141 observations of PM_{2.5}, PM₁₀, O₃, NO_x, CO and SO₂ concentrations in the three selected regions in both
142 winter and summer conditions (specifically for January and July 2010). During wintertime, stable and
143 stagnant conditions, occurring in particular in northern China, constitute a favorable environment for the
144 accumulation of pollutants, and lead to persistent haze events. Photochemical activity, which increases
145 during summertime, leads to enhanced ozone concentrations.

146 The specific objectives of the present study are (1) to assess the ability of the selected WRF-Chem
147 configuration (see Sect. 2.1) to reproduce the distributions and concentrations of pollutants in Eastern
148 China in both summer and winter conditions, (2) to investigate the ability of the model to capture
149 specific pollution events under specific meteorological conditions, (3) to investigate the air quality

150 responses to changes in emissions through sensitivity studies to anthropogenic emission inventories, (4)
151 to identify shortcomings that need to be addressed to improve the air quality model predictions.
152 A detailed description of the selected WRF-Chem configuration and of the evaluation datasets are given
153 in Section 2. Section 3 presents an evaluation of the representation of meteorological situations by the
154 model. A comparison of the HTAPv2, REASv2 and MACCity anthropogenic emission inventories and
155 an evaluation of their influence on simulated spatial distributions of pollutants are presented in Section
156 4. The model simulations are evaluated against surface measurements of pollutants in Section 5. Section
157 6 presents a summary and conclusions of the present work and suggestions for future research activities.

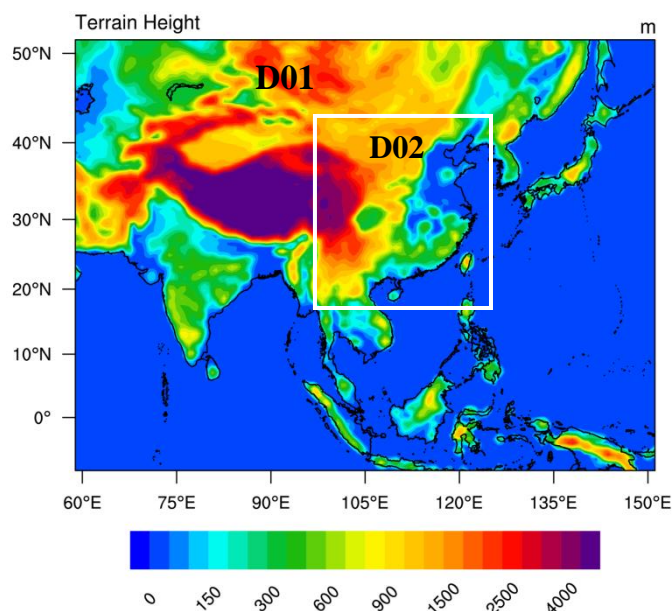
158 **2. Model description and evaluation datasets**

159 **2.1 Model configuration**

160 WRF-Chem is the Weather Research and Forecasting (WRF) model (Skamarock et al., 2008) coupled
161 to chemistry (Grell et al., 2005; Fast et al., 2006). For this study, we used version 3.6.1 to simulate the
162 meteorology and chemistry simultaneously in the model domains shown on Figure 1. Domain D01 with
163 60 km horizontal grid spacing extends from India to the Pacific Ocean and from Malaysia to southern
164 Russia to cover the most polluted areas in Asia. Domain D02 covers the eastern part of China with a 20
165 km grid resolution. The vertical grid is composed of 51 levels extending from the surface to 10 hPa
166 (~30 km) with a spacing of about 40-50 m near the surface, 200–450 m for altitudes around 1–3 km and
167 500–700 m for altitudes between 4 and 14 km. The resolved scale cloud physics is represented by the
168 Thompson microphysics scheme (Thompson et al., 2004, 2008) and sub-grid scale effects of convective
169 and shallow clouds are parameterized according to Grell and Freitas (2014). The short- and long-wave
170 radiative transfer in the atmosphere are represented by the Goddard scheme (Chou et al., 1998) and the
171 Rapid Radiative Transfer Model (RRTM) (Mlawer et al., 1997) respectively. For surface processes, the
172 model setup uses the NOAH land-surface model (Chen and Dudhia, 2001) and the revised MM5
173 Monin-Obukhov surface layer scheme. The vertical sub-grid scale fluxes due to eddy transport in the
174 planetary boundary layer (PBL) and the free troposphere are parameterized according to the Yonsei
175 University (YSU) boundary layer scheme (Hong et al., 2006).

176 The gas-phase chemistry is represented by the Model for Ozone and Related Chemical Tracers
177 (MOZART-4) chemical scheme (Emmons et al., 2010). The Goddard Chemistry Aerosol Radiation and
178 Transport (GOCART) aerosol module coupled with MOZART is used in this study to take into account

179 the aerosol processes. GOCART is a bulk aerosol model (Chin et al., 2002; Ginoux et al., 2001) and
180 provides total mass information on sulfate, organic and black carbon, PM_{2.5} and PM₁₀. It includes also a
181 sectional scheme for dust (5 bins) and sea salt (4 bins). The GOCART model is numerically efficient
182 and useful for process studies focused on both gas phase and aerosol chemistry. The model
183 configuration used in this study, with the exception of the GOCART aerosol scheme, which has been
184 replaced by the MOSAIC scheme (Zaveri et al., 2008), was successfully implemented to provide daily
185 operational air quality forecasts in China, available at <http://www.marcopolo-panda.eu>.



186
187
188
189
190
191
192
193
194
195
196
197
198
199
Figure 1: Terrain height (m) over East Asia and
WRF-Chem model domain settings.

200 2.2 Model input datasets

201 The initial and lateral boundary conditions for the meteorological variables are obtained from the
202 National Center for Environmental Predictions and Final Analysis (NCEP-FNL) available every 6 hours
203 at 1°×1° spatial resolution. For the chemical and aerosol species, initial and lateral boundary conditions
204 are provided by the global operational forecasting system implemented within the EU MACC (now
205 CAMS, <https://atmosphere.copernicus.eu>) project (Flemming et al., 2009, 2015). The MACC system is
206 constrained by assimilation of CO, O₃ and NO₂ observations from several satellite instruments using the
207 ECMWF 4D-Var assimilation system (Inness et al., 2013). This makes the MACC products, which are

208 also based on the MOZART model, ideal for use in regional coupled models. Missing species in the
209 MACC datasets, such as some VOCs, are provided by the MOZART-4 global model forecasts
210 performed routinely at the National Center for Atmospheric Research (NCAR)
211 (<http://www.acom.ucar.edu/wrf-chem/mozart.shtml>). This model includes a detailed formulation of
212 VOC speciation and aerosol concentrations (Emmons et al., 2010). Both MACC/CAMS and MOZART-
213 4 chemical data forecasts are frequently used to derive several regional air quality forecasting systems
214 across the world with initial and lateral boundary conditions.

215 As mentioned in the previous sections, three anthropogenic emissions inventories are considered in this
216 study. The HTAPv2 emissions inventory consists of $0.1^\circ \times 0.1^\circ$ gridmaps of several species including
217 CO, SO₂, NO, NMVOC, NH₃, BC and OC for the years 2008 and 2010. The dataset is available on the
218 ECCAD data portal (<http://eccad.aeris-data.fr>). It has been constructed using nationally reported
219 emissions combined with regional scientific inventories in the format of sector-specific gridmaps. For
220 China, it includes the Multi-resolution Emission Inventory for China (MEIC), which is available at
221 <http://www.meicmodel.org>. Detailed description and qualitative assessment of the HTAPv2 emissions
222 are provided in Janssens-Maenhout et al. (2015).

223 The REASv2.1 inventory has been developed since 2007 for the analysis of long-term trends of the
224 Asian atmospheric environment (Kurokawa et al., 2013). This dataset includes most major air pollutants
225 and greenhouse gases for the following areas in Asia: East, Southeast, South, and Central Asia and the
226 Asian part of Russia. Monthly gridded data with a $0.25^\circ \times 0.25^\circ$ resolution are provided for the major
227 emissions sectors and are available at <http://www.nies.go.jp/REAS/>.

228 MACCity is a global emissions inventory developed in the framework of the European MACC and
229 CityZen projects. It provides emissions of several species including CO, NO_x, SO₂, NH₃, OC and BC
230 and NMVOC (Granier et al., 2011). The monthly gridded emission data with a resolution of $0.5^\circ \times 0.5^\circ$
231 for the major sectors are available on the ECCAD web portal.

232 Three WRF-Chem simulations, hereafter named HTP, RAS and MCT, using separately the emissions
233 HTAPv2, REASv2 and MACCity, respectively, are performed and analysed in this study. In addition to
234 anthropogenic emissions, daily varying emissions of trace species from biomass burning were taken
235 from the Fire Inventory from NCAR version 1 (FINN v1) (Wiedinmyer et al., 2011). They are
236 distributed vertically in the model following the online plume-rise module (Freitas et al., 2007).
237 Biogenic emissions of trace species from terrestrial ecosystems are calculated online using the Model of

238 Emissions of Gases and Aerosols from Nature (MEGAN) version 2.04 (Guenther et al., 2006). Dust
239 and seas salt are simulated using the GOCART emission scheme (Ginoux et al., 2001).

240

241 **2.3 Observational datasets and evaluation methodology**

242 For the evaluation of the model performance, satellite data as well as surface measurements made
243 available within the PANDA project are used to assess both the spatial distribution and temporal
244 variation of pollutants. Evaluation of the spatial patterns is performed by comparing the simulated total
245 CO columns and tropospheric NO₂ columns against MOPITTv6 (Deeter et al., 2014) and GOME2
246 (Callies et al., 2000; Boersma et al., 2004) satellite observations respectively. Evaluation of the
247 temporal variations is conducted using ground-based measurements of meteorological fields as well as
248 chemical and aerosol species in Beijing, Shanghai and Guangzhou in January and July 2010. The
249 meteorological datasets include surface temperature, wind speed and direction, relative humidity and
250 precipitation. The chemical and aerosol species include NO_x, O₃, CO, SO₂, PM_{2.5} and PM₁₀. For a
251 comprehensive model evaluation in each region, the following statistical indicators that provide
252 complementary and valuable information on the model performance have been calculated: the mean
253 bias (MB), the mean fractional bias (MFB), the mean fractional error (MFE), the root mean square error
254 (RMSE), the correlation coefficient (*R*) and the index of agreement (IOA). These validation metrics are
255 described in many publications (Kang et al. 2006; Wilks, 2006; Willmott et al. 2012; Brasseur and
256 Jacob, 2017) and are used in several model evaluation studies (e.g. Fu et al., 2012; Eskes et al., 2015)
257 including the evaluation of the MACC European ensemble air quality forecasts (Marécal et al., 2015).
258 They are computed using the following formulas:

$$MB = \frac{1}{N} \sum_i (m_i - o_i)$$

$$MFB = \frac{2}{N} \sum_i \frac{m_i - o_i}{m_i + o_i}$$

$$MFE = \frac{2}{N} \sum_i \frac{|m_i - o_i|}{m_i + o_i}$$

$$RMSE = \sqrt{\frac{1}{N} \sum_i (m_i - o_i)^2}$$

$$R = \frac{\frac{1}{N} \sum_i (m_i - \bar{m}) (o_i - \bar{o})}{\sigma_m \sigma_o}$$

259

$$IOA = \begin{cases} 1 - \frac{\sum_i |m_i - o_i|}{2 \sum_i |o_i - \bar{o}|}, & \text{if } \sum_i |m_i - o_i| \leq 2 \sum_i |o_i - \bar{o}| \\ \frac{2 \sum_i |o_i - \bar{o}|}{\sum_i |m_i - o_i|} - 1, & \text{if } \sum_i |m_i - o_i| > 2 \sum_i |o_i - \bar{o}| \end{cases}$$

260

261 The ensemble N consists of paired model and observed quantities m_i and o_i , whose averages are \bar{m} and
 262 \bar{o} and standard deviations are σ_m and σ_o .

263

264 **3. Meteorology evaluation**

265 Simulated daily mean surface temperature, wind speed and direction, relative humidity and precipitation
 266 are compared with surface observations made available within the PANDA project in the three
 267 considered cities. In Beijing, the temperature decreased to around -15 °C on the 5th of January 2010 and
 268 started to increase afterwards but remained almost negative during the whole month of January. Only
 269 one moderate precipitation event (1.7 mm) was observed on the 3rd of January (not shown), while the
 270 relative humidity exhibited a considerable temporal variability. Overall, WRF-Chem predicted
 271 temperature and relative humidity agree very well with the observations in Beijing in January 2010.
 272 During the month of July 2010, the observed temperature values exceeded 23 °C and the relative
 273 humidity remained around 70-80% except during the first week of July when it dropped to less than
 274 40%. WRF-Chem predicted temperature and relative humidity for July agree also very well with the
 275 observations although relative humidity is underestimated by around 10%. The simulated pattern for
 276 wind speed agrees better with the observations in January than in July. The model tends however to
 277 overpredict the observed maximum values in Beijing.

278 The meteorological observations in Shanghai (Figure 3) show positive temperature values in January,
 279 being higher than in Beijing, and observed relative humidity varies between 40 to 90%. In July,
 280 recorded temperature varies between 25°C and 33°C and relative humidity remained higher than 60%.
 281 WRF-Chem predicted temperature and relative humidity agree very well with the observations in
 282 January. Predicted values in July 2010 are also in good agreement with the observations although

283 simulated temperature is slightly lower by around 1 to 2°C and relative humidity is higher by around
 284 10% in the model during some specific days. As in Beijing, the model tends to overpredict maximum
 285 mean wind speed by up to 2 m s⁻¹ in January and 4 m s⁻¹ in July 2010. The general pattern of the
 286 simulated wind direction agrees well with the observations in January but a better agreement is found in
 287 July 2010.

288

289

290

291

292

293

294

295

296

297

298

299

300

301

302

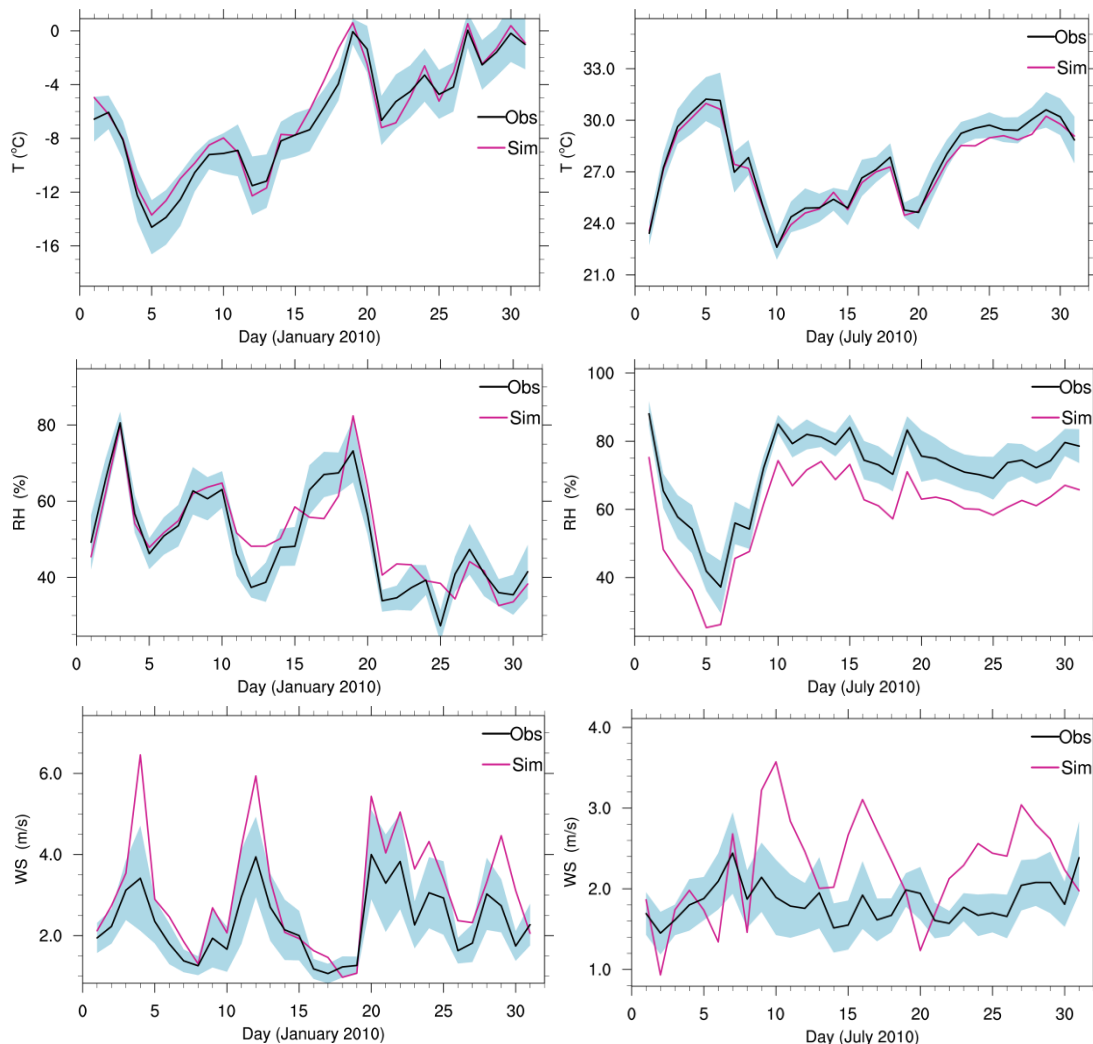
303

304

305

306

307



308 Figure 2: Time series of observed (black) and simulated (red) daily mean temperature (T),
 309 relative humidity (RH), wind speed (WS) in Beijing for January (left panels) and July (right
 310 panels) 2010. Standard deviations from the mean observations indicated with shaded area.

310

311

312

313

314

315

316

317

318

319

320

321

322

323

324

325

326

327

328

329

330

331

332

333

334

335

336

337

338

339

340

341

342

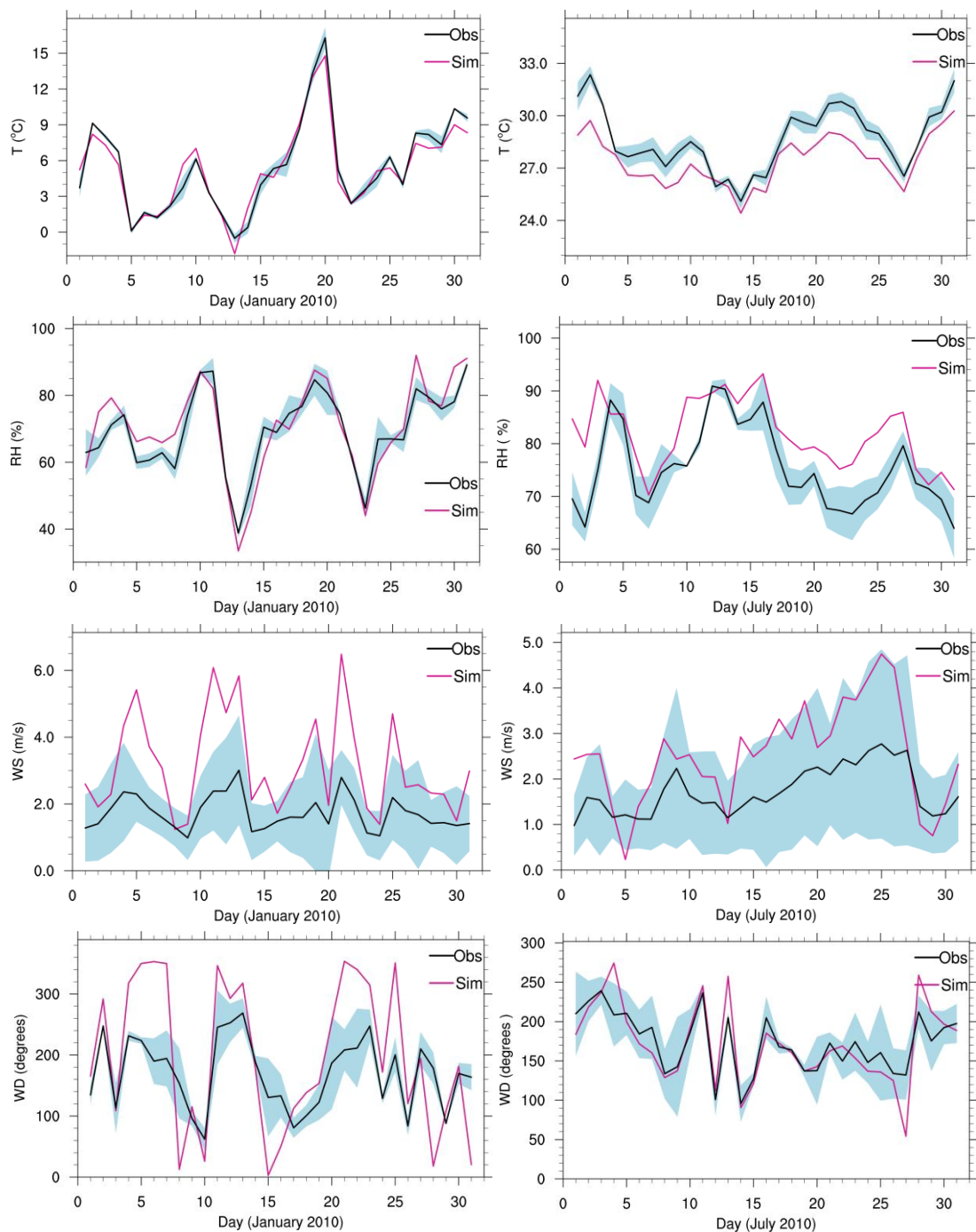


Figure 3: Time series of observed (black) and simulated (red) daily mean temperature (T), relative humidity (RH), wind speed (WS) and wind direction (WD) in Shanghai for January (left panels) and July (right panels) 2010. Standard deviations from the mean observations indicated with shaded area.

343

344

345

346

347

348

349

350

351

352

353

354

355

356

357

358

359

360

361

362

363

364

365

366

367

368

369

370

371

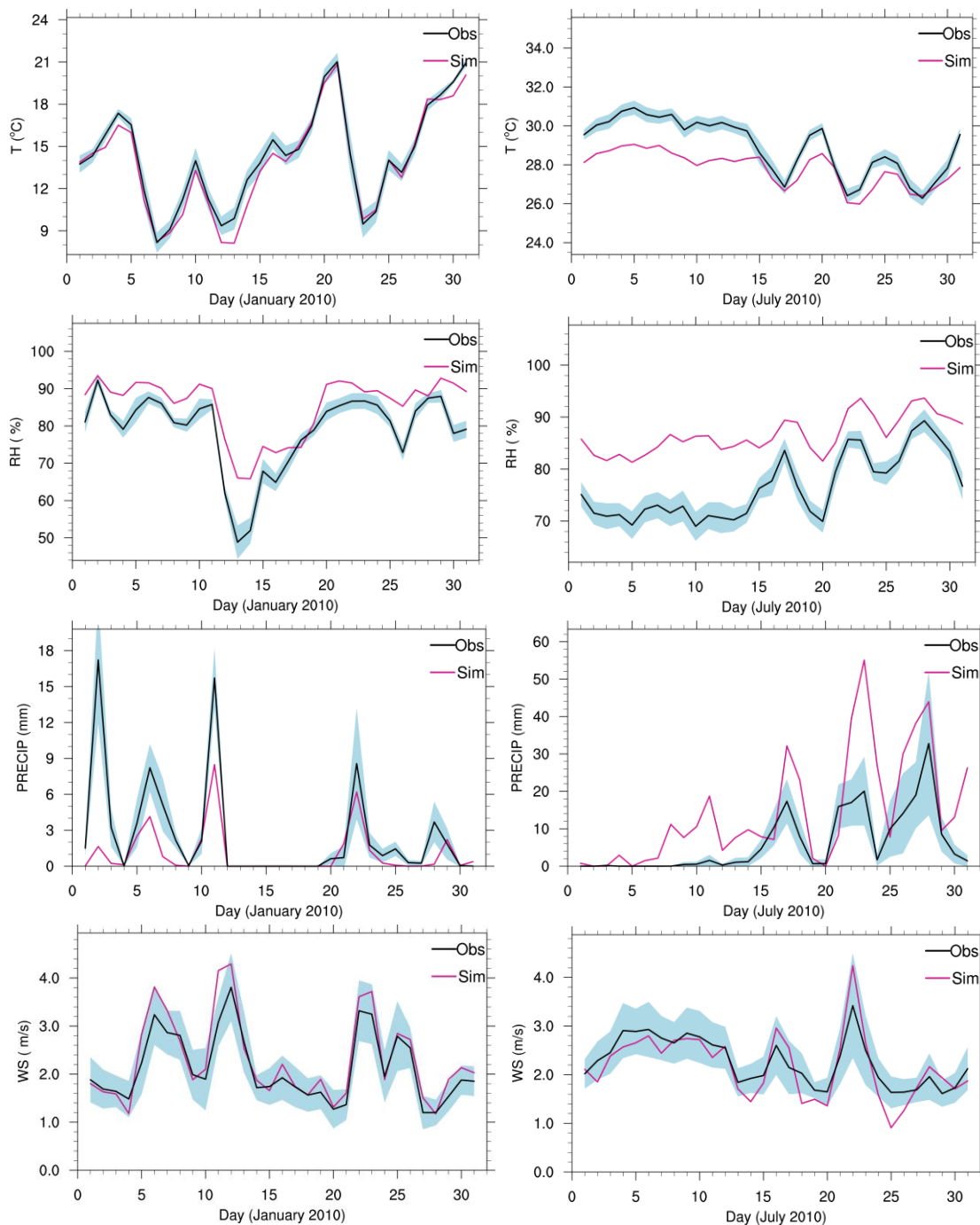


Figure 4: Time series of observed (black) and simulated (red) daily mean temperature (T), relative humidity (RH), precipitation (PRECIP) and wind speed (WS) in Guangzhou for January (left panels) and July (right panels) 2010. Standard deviations from the mean observations indicated with shaded area.

372 In Guangzhou, the observed variability of temperature, wind speed, temperature and relative humidity
373 in January 2010 are well captured by the model (Figure 4). Predicted temperature is almost similar to
374 the observations while wind speed and relative humidity are slightly higher (by around 1m/s and less
375 than 15% respectively). The model captures nicely the precipitation events in January but observed peak
376 values are underestimated. Predicted temperature and wind speed in July 2010 show also good
377 agreement with observations although simulated temperature values are slightly lower. The model tends
378 to overpredict both RH (+15%) and precipitation (by 10-40 mm) in July 2010.

379 Overall, the WRF-Chem model setup used in the current study satisfactorily reproduces the
380 meteorological situation in the three cities, allowing a better and confident analysis of the air quality
381 model results discussed in the following sections. This is despite some overestimations of maximum
382 values of surface wind speed which have also been reported in previous WRF-Chem modelling studies
383 (Zhang et al. 2010; Tuccella et al. 2012; Zhang et al. 2015). Unresolved topographic features due to the
384 smoother topography used in the model are among the possible reasons for the surface wind speed issue
385 in WRF-Chem (Jiménez and Dudhia, 2012).

386

387 **4. Overview on the impact of emissions on model results**

388 In this section we compare first the three anthropogenic emission inventories HTAPv2, REASv2 and
389 MACCity to assess their differences in both spatial distributions and magnitude of emissions. The three
390 WRF-Chem simulations HTP, RAS and MCT, using separately these three different emission
391 inventories are then analysed and compared with satellite measurements in order to assess the impact of
392 anthropogenic emissions on air quality model predictions.

393

394 **4.1 Comparison of the anthropogenic emissions**

395 In order to quantify the differences between the inventories, averages of the emissions have been
396 calculated over the domain D02 and also over three selected different city clusters, which include
397 Beijing (the so-called Hebei-Beijing-Tianjin region), Shanghai (the Yangtze River Delta) and
398 Guangzhou (the Pearl River Delta). The Tables 1 and 2 show the HTAPv2 total emissions of CO, NO,
399 SO₂, BC and OC in January and July respectively, and the percentage differences between the HTAPv2
400 estimates and those of MACCity and REASv2. In January, HTAPv2 emissions are generally higher
401 than those of MACCity in the domain D02 but lower estimates are found in some regions and for some

402 species. For example, while HTAPv2 estimates are higher Beijing than those of MACCity, with large
 403 differences found for CO, BC and OC (98%, 60% and 85% respectively), they are lower in Guangzhou.
 404 HTAPv2 emissions of CO, NO and OC are also higher in Shanghai (17%, 30% and 10% respectively),
 405 while lower estimates are provided for SO₂ and BC (-40% and -15% respectively). The HTAPv2
 406 estimates for CO, NO and SO₂ are generally lower in the considered domain and regions when
 407 compared to REASv2. HTAPv2, presents however higher BC and OC emissions in the domain D02 and
 408 in Beijing, but lower estimates in Guangzhou.

409

410

411

Table 1: Total anthropogenic emissions in January in HTAPv2 in model domain D02 and in the Beijing, Shanghai and Guangzhou city-clusters and percentage differences with MACCity and REASv2.

		CO	NO	SO ₂	BC	OC
D02	HTAPv2 (Tg/month)	21.3	1.6	2.64	0.23	0.54
	HTAPv2-MACCity (%)	37	12	-4.7	27.8	54.3
	HTAPv2-REASv2 (%)	-20.4	-7	-4.7	9.5	25.6
Beijing	HTAPv2 (Tg/month)	3.87	0.27	0.41	0.037	0.074
	HTAPv2-MACCity (%)	98.5	35	7.9	60.9	85
	HTAPv2-REASv2 (%)	-28	-	-6.8	15.6	34.5
Shanghai	HTAPv2 (Tg/month)	2.47	0.26	0.24	0.022	0.054
	HTAPv2-MACCity (%)	17	30	-40	-15.4	10.2
	HTAPv2-REASv2 (%)	-39.8	-10.3	-17.2	-18.5	8
Guangzhou	HTAPv2 (Tg/month)	0.7	0.086	0.12	0.006	0.016
	HTAPv2-MACCity (%)	-44	-28	-48	-65	-45
	HTAPv2-REASv2 (%)	-54.5	-28	-25	-40	-30

412

413

414

415

416

417

418

419

420

421

422

423

424

425

426

427

428

429

430

431

432

433

434

435

436

437

438

439

440

441

442

443

444

445

446

447

448

449

450

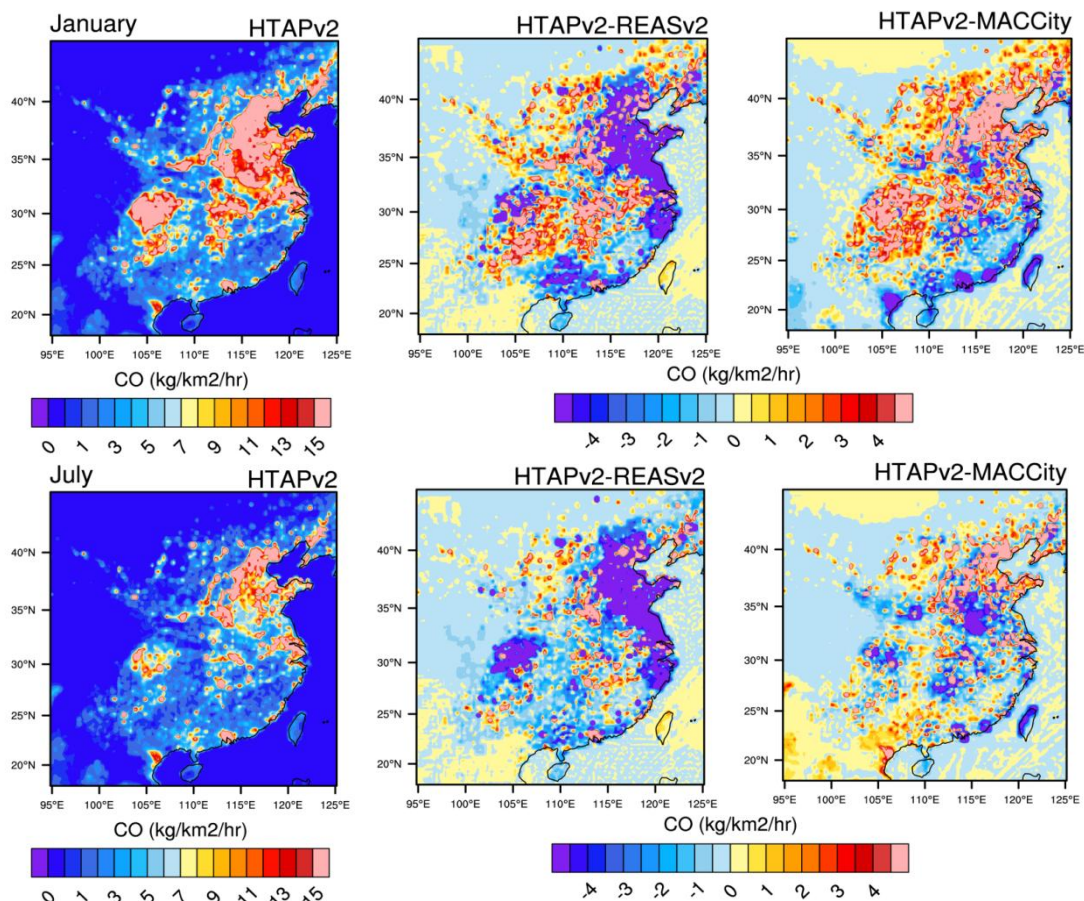


Figure 5: CO anthropogenic emissions ($\text{Kg}/\text{km}^2/\text{hr}$) in January (top panel) and July (bottom panel) in HTAPv2 and absolute differences with RASv2 and MACCity emissions.

In July, HTAPv2 estimates are also generally higher than those of MACCity in the domain D02 and in Beijing, where differences of up to 78%, 86% and 42% are found in CO, NO and SO_2 emissions respectively. HTAPv2 CO and NO_x emissions are also higher than those of MACCity in Shanghai (23% and 80% respectively) but only moderate differences are found in Guangzhou. The larger differences in this region are found in BC and OC emissions (-40% and 45% respectively). As in January, HTAPv2 estimates are lower than those of REASv2 for many of species and large differences are found in CO and BC emissions (e.g. -53% and -35% respectively in Shanghai).

451

Table 2: Total anthropogenic emissions in July in HTAPv2 in model domain D02 and in the Beijing, Shanghai and Guangzhou city-clusters and percentage differences with MACCity and REASv2.

452

453

		CO	NO	SO ₂	BC	OC
D02	HTAPv2 (Tg/month)	11.56	1.57	2.3	0.11	0.19
	HTAPv2-MACCity (%)	19.2	42.7	24.2	-	35.7
	HTAPv2-REASv2 (%)	-40.9	-7.1	-14.8	-21.4	-9.5
Beijing	HTAPv2 (Tg/month)	2.2	0.28	0.37	0.018	0.024
	HTAPv2-MACCity (%)	78.9	86.7	42.3	28.6	41.2
	HTAPv2-REASv2 (%)	-46.8	12	-5.1	-21.7	-20
Shanghai	HTAPv2 (Tg/month)	1.55	0.27	0.26	0.013	0.02
	HTAPv2-MACCity (%)	23	80	-3.7	-13.3	5.3
	HTAPv2-REASv2 (%)	-53.7	-10	-16.1	-35	-23.1
Guangzhou	HTAPv2 (Tg/month)	0.71	0.096	0.14	0.006	0.016
	HTAPv2-MACCity (%)	-5.3	6.7	-6.7	-40	45.5
	HTAPv2-REASv2 (%)	-40.8	-12.7	-12.5	-25	6.7

454

455

456

457

458

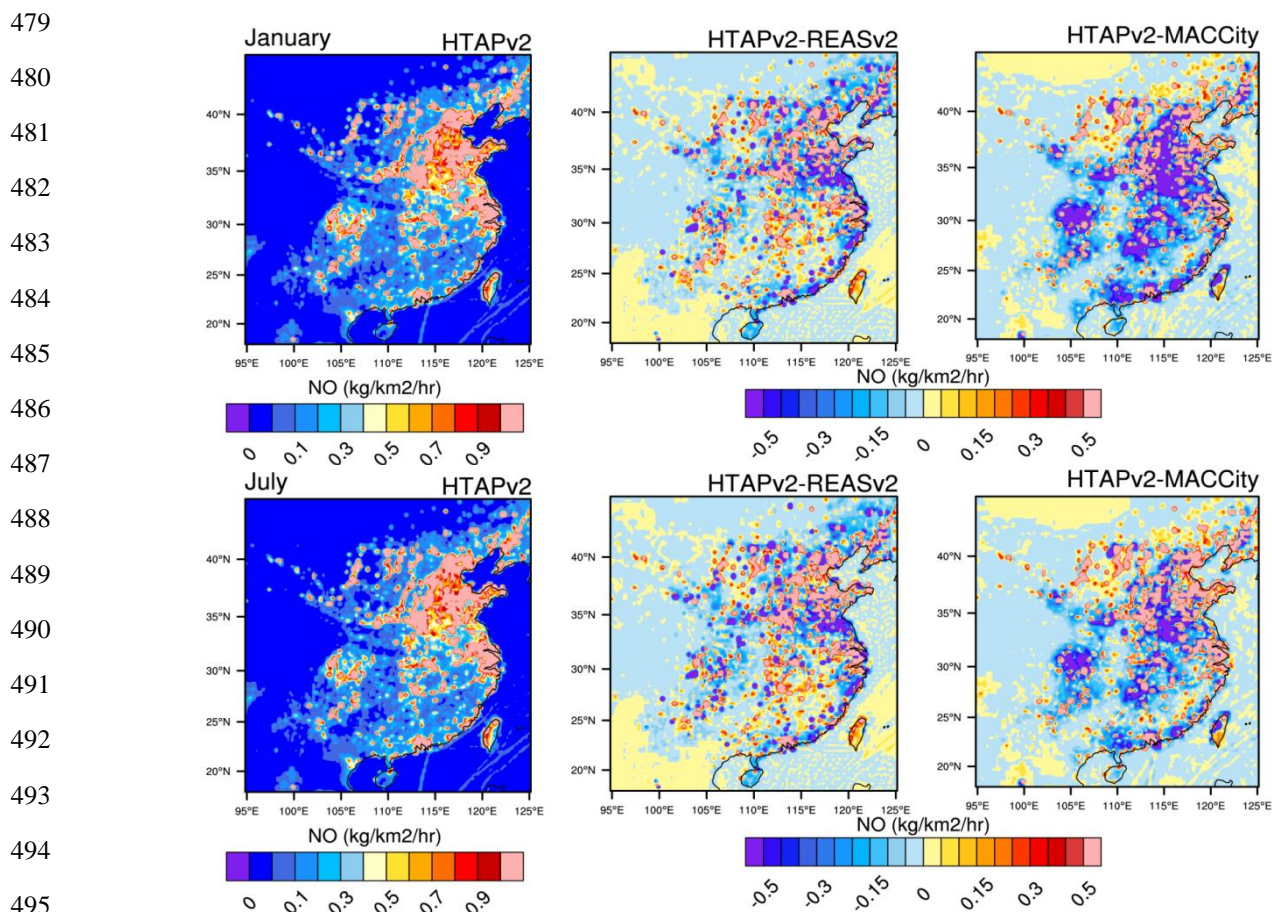
459

460

461 In order to illustrate differences in the spatial distributions of the emissions, Figures 5 and 6 display
 462 monthly mean CO and NO emission fluxes in January and July from the HTAPv2 inventory and the
 463 calculated absolute differences with REASv2 and MACCity. Consistent with the results in Tables 1 and
 464 2, CO emissions in HTAPv2 are lower than in REASv2 in Beijing and the north-eastern regions in both
 465 January and July. HTAPv2 exhibits also lower CO fluxes in the Sichuan Basin in July, but generally
 466 higher estimates in central China in January. The HTAPv2 CO emissions are generally higher compared
 467 to MACCity in central and northern China in January, but lower in the south-coastal regions. The
 468 differences between HTAPv2 and REASv2 NO emissions at the regional scale are small, particularly in
 469 January, but large discrepancies can be found in specific cities and local areas. Large differences
 470 between HTAPv2 and MACCity NO emissions can be seen in several regions, in particular in the
 471 northern and central regions of China.

472 Overall, the differences between the three inventories in terms of magnitude, resolution and spatial
 473 distribution of the emissions are clearly visible at both the provincial and city scales. Large differences
 474 are found over some specific areas such as the north-east region, the south coasts and central regions of

475 China, in particular for some specific species (e.g. CO and NO). The magnitude of the differences
 476 between the emissions estimates are not uniformly similar between January and July, and depend also
 477 on the species and regions considered. This indicates that in addition to differences in the resolution and
 478 spatial distribution of the emissions, there are also differences in their temporal variations.



496 Figure 6: NO anthropogenic emissions ($\text{Kg}/\text{km}^2/\text{hr}$) in January (top panel) and July
 497 (bottom panel) in HTAPv2 and absolute differences with RASv2 and MACCity emissions.

498

499 **4.2 Effect of anthropogenic emissions on spatial distribution of pollutants**

500 In this section we compare the WRF-Chem simulations HTP, RAS and MCT, conducted separately
 501 with the HTAPv2, REASv2 and MACCity emissions respectively described in Section 2.3, to assess the
 502 changes in air quality model predictions related to the differences in the emissions. Figure 7 shows
 503 monthly mean surface mixing ratios of CO, NO_x and O₃, and PM_{2.5} concentrations in January from the
 504 HTP simulation and absolute differences with RAS and MCT predictions.

505

506

507

508

509

510

511

512

513

514

515

516

517

518

519

520

521

522

523

524

525

526

527

528

529

530

531

532

533

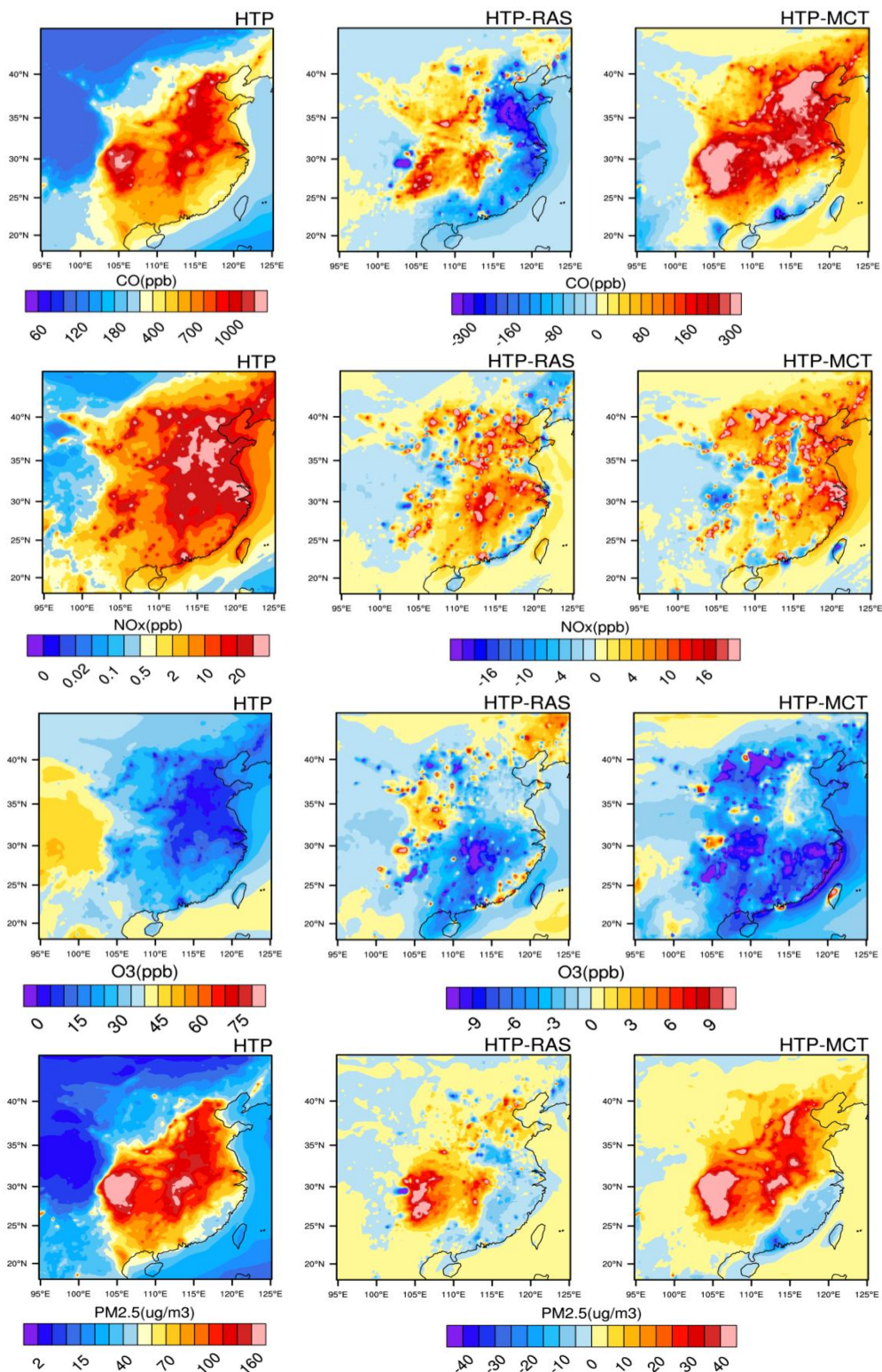


Figure 7: Monthly mean surface CO, NO_x, O₃ and PM_{2.5} surface concentrations simulated for January 2010 using HTAPv2 emissions (HTP) and absolute differences with model predictions with REASv2 (RAS) and MACCity (MCT) emissions.

534 The most polluted regions in wintertime (>1 ppm, >50 ppb and $>120 \mu\text{g m}^{-3}$ of CO, NO_x and PM_{2.5}
535 respectively) are located in north-eastern China, and in the Sichuan and Guangdong provinces, which
536 are located in central and southern China respectively. Predicted CO concentrations for January are
537 higher in RAS by more than 200 ppb compared to HTP in most of the north-eastern part of the country
538 and around the coastal regions as a consequence of higher CO emissions in the REASv2 inventory (see
539 Table 1). In central China however, HTP predicted higher concentration than RAS (over 100 ppb). This
540 is again consistent with the differences in CO emissions identified between HTAPv2 and REASv2
541 inventories on Figure 5. In comparison to MCT, the HTP simulation shows higher CO values in most
542 regions except in the Guangzhou region and other south coastal areas where MCT predicted CO
543 concentrations higher by more than 150 ppb. This is also directly linked to differences in the emissions
544 since, as indicated on Table 1 (see also Figure 5), HTAPv2 CO emissions estimates are higher than that
545 of MACCity in Beijing and Shanghai regions, but lower in Guangzhou.

546 The general patterns of the differences in simulated NO_x concentrations in January exhibit also
547 similarities with those of the emissions. HTP predicted up to 10-15 ppb lower concentrations compared
548 to RAS in the south coastal regions, but higher values in the central and northern regions. It predicted
549 also more than 15 ppb higher NO_x concentrations compared to MCT in most parts of China,
550 particularly in the north-eastern regions. The predicted O₃ concentrations over these regions are
551 relatively low in January due to (1) low photochemical activity and (2) very high NO_x concentrations,
552 which does not favour the build-up of O₃ due to titration effects. This could explain why HTP predicts
553 lower O₃ concentrations in general (by up to 10 ppb) compared to MCT over most regions. Similarly,
554 differences in the predicted O₃ between HTP and RAS could also be linked to differences in the
555 predicted NO_x concentrations.

556 In the case of PM_{2.5}, HTP shows concentrations slightly lower by approximately $15 \mu\text{g m}^{-3}$ compared to
557 MCT in Guangzhou and other southern parts of China due to lower BC and OC emissions in the
558 HTAPv2 inventory (see Table 1). PM_{2.5} concentrations higher by more than $30 \mu\text{g m}^{-3}$ are simulated,
559 however, in the Sichuan province in central China. The differences in PM_{2.5} between HTP and RAS do
560 not exceed $15 \mu\text{g m}^{-3}$ in general in most regions except in the Sichuan province where HTP predicts
561 higher concentrations by more than $30 \mu\text{g m}^{-3}$.

562

563

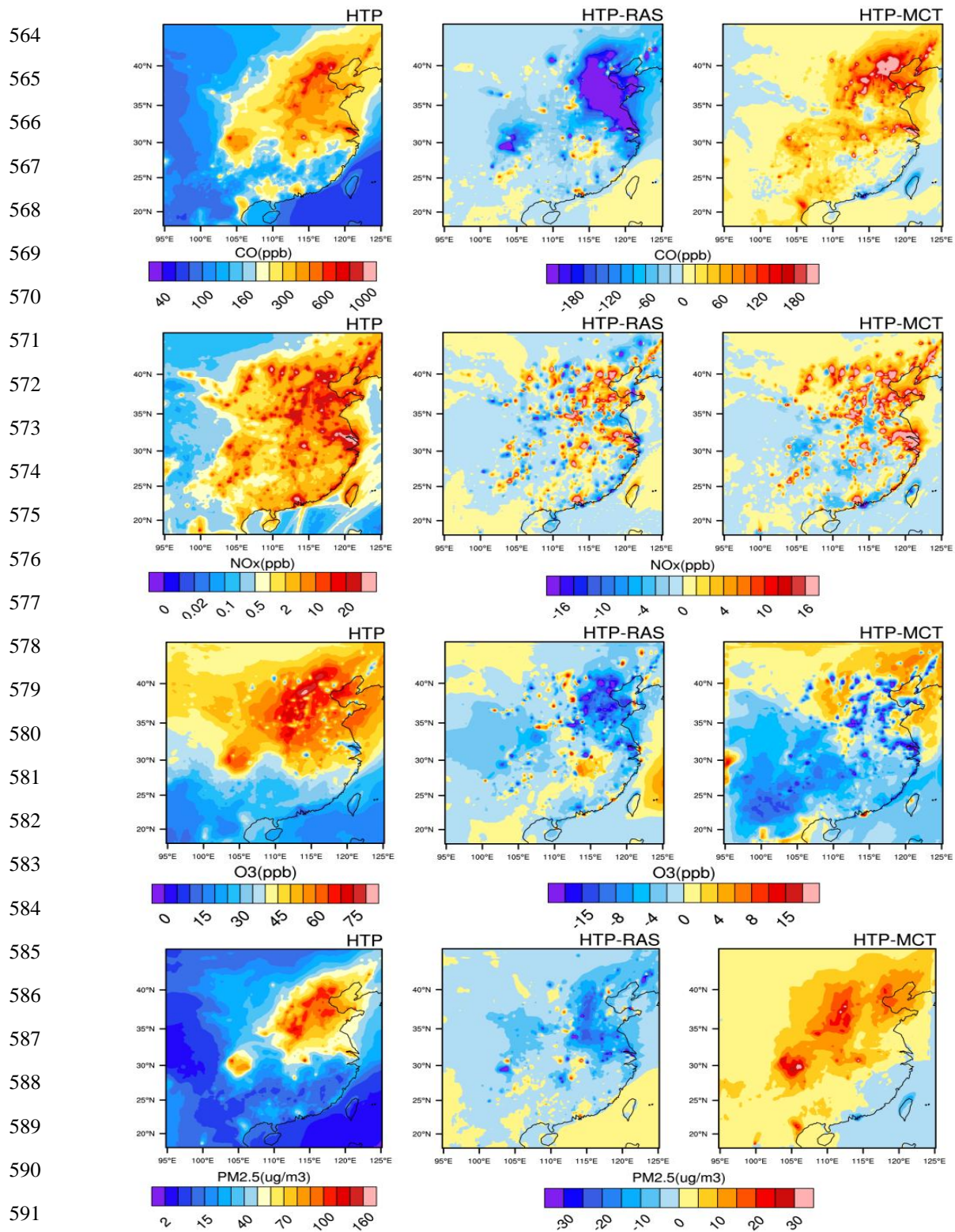


Figure 8: Monthly mean surface CO, NO_x, O₃ and PM_{2.5} surface concentrations simulated for July 2010 using HTAPv2 emissions (HTP) and absolute differences with model predictions with REASv2 (RAS) and MACCity (MCT) emissions.

594 Figure 8 illustrates the results and differences for July 2010. The highest CO, NO_x and PM_{2.5}
595 concentrations are found mostly in the northern regions. Predicted concentrations are however lower
596 (<500 ppb, <50 ppb and <100 µg m⁻³ respectively) compared to those in January due to a combination
597 of lower emissions, increased photochemical activity during summer and increased precipitation due to
598 the Asian monsoon, which increases the removal of soluble species. There are also clear similarities in
599 the patterns of the differences between the simulations and those of the emissions in July. The HTP
600 simulation predicts CO and NO_x concentrations that are higher by more than 100 ppb and 10 ppb
601 respectively compared to MCT in the north-eastern regions. HTP shows also higher NO_x compared to
602 RAS over the north-eastern regions but lower CO concentrations (by more than 15 ppb and less than
603 200 ppb respectively). This is also consistent with the differences between HTAPv2 and REASv2
604 concerning the NO and CO emissions as indicated on Figures 5 and 6 respectively. The differences in
605 O₃ between the simulations do not exceed 10 ppb in most regions in general, but higher differences of
606 more than 15 ppb can be found in some specific regions such as Beijing and Shanghai and surrounding
607 areas. The HTP simulation shows PM_{2.5} concentrations up to 20 µg m⁻³ lower than RAS in the northern
608 regions, but over 20 µg m⁻³ higher values compared to MCT. Again, these discrepancies could be
609 related to the differences between the emissions estimates such as for BC and OC.

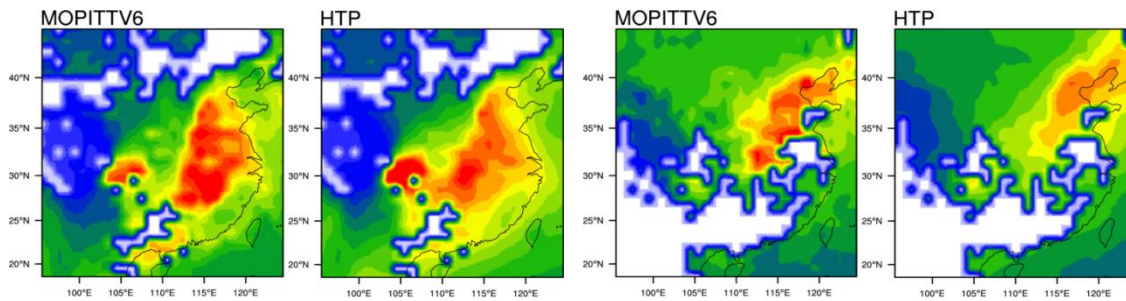
610

611 **4.3 Comparison with satellite observations**

612 The spatial distribution of pollutants and the effects of anthropogenic emissions are also assessed in this
613 section by comparing results of the three model simulations HTP, RAS and MCT with MOPITTv6 and
614 GOME2 satellite observations. Comparisons of the simulated CO total columns for January and July
615 2010 against MOPITTv6 CO retrievals are shown on Figure 9. For an appropriate comparison, modeled
616 CO concentrations are transformed by the MOPITTv6 averaging kernels and a priori CO profiles.
617 Details on the method of calculation can be found in Wagner et al. (2015) and references therein.

618 In general, the HTP and RAS simulations exhibit almost similar CO distributions in January and higher
619 concentrations than MCT due to higher CO emissions in the HTAPv2 and REASv2 inventories
620 compared to MACCity as discussed in Sect. 4.1 (see also Table 1). The model simulations are generally
621 consistent with MOPITTv6 observations, capturing correctly the spatial patterns of CO total columns,
622 and the high values in eastern China and in the Sichuan basin. There are however some differences with
623 MOPITTv6 regarding the magnitude of CO total columns.

624



625

626

627

628

629

630

631

632

633

634

635

636

637

638

639

640

641

642

643

644

645

646

647

648

649

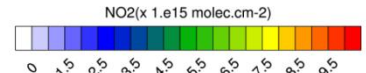
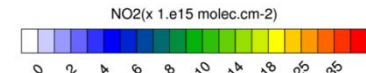
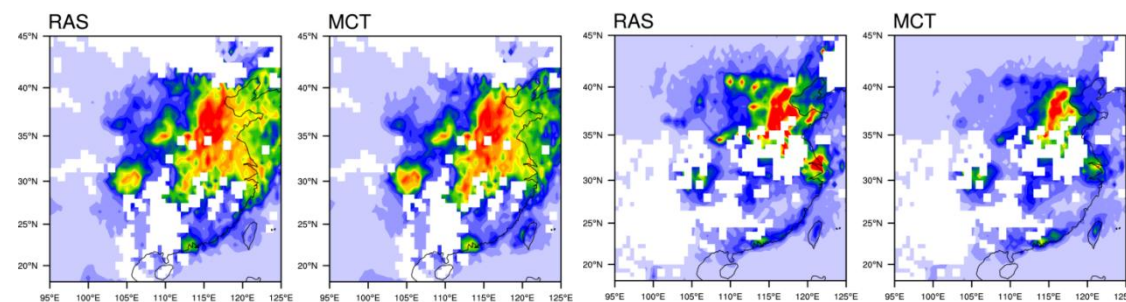
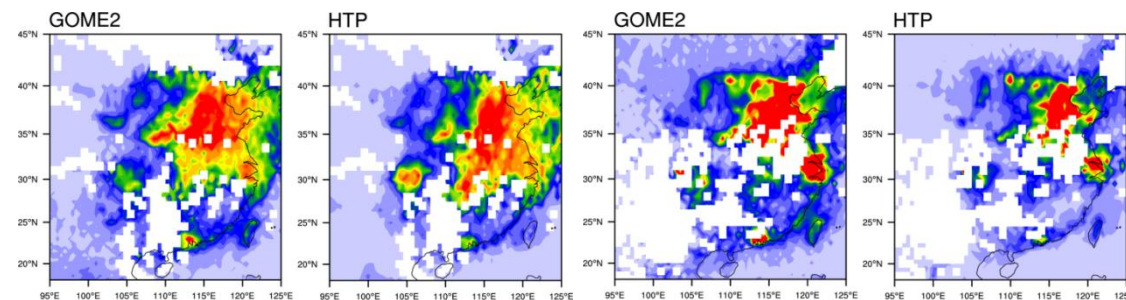
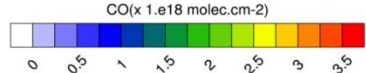
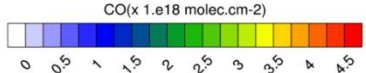
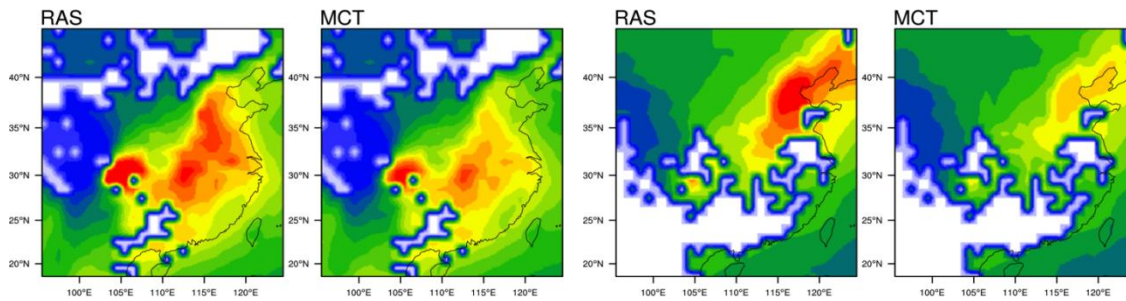


Figure 9: Comparison of predicted CO total columns and NO₂ tropospheric columns in January (left panels) and July 2010 (right panels) with the three emissions inventories against MOPITTv6 and GOME2 observations, respectively.

650

651

652

653

654 All the simulations tend to underestimate the high CO concentrations in eastern China in January
655 although RAS and HTP show higher values over the Sichuan province compared to MOPITTv6.
656 Comparisons with surface CO measurements in the Beijing region discussed in Sect. 5.1 also lead to the
657 same conclusion of CO underestimation in the simulations in January 2010, although observations are
658 available only at one station. Underestimation of wintertime CO emissions in some eastern China
659 provinces in the current inventories could be a possible explanation for the CO underestimation in the
660 model simulations. Stein et al. (2014) pointed also to possible overestimation of CO sinks (e.g. dry
661 deposition) in most state-of-the-art chemistry transport models, which can lead the negative CO bias in
662 the northern hemisphere during winter.

663 The regions of high CO concentrations in July 2010 are located in north-eastern China, especially in the
664 Beijing region, while the southern regions, influenced by the summer Asian monsoon, show lower CO
665 concentrations. The general spatial pattern of CO total columns in July is well captured by the
666 simulations, which show however significant magnitude differences related to the differences between
667 the applied emissions. Predicted CO values in July are higher in RAS than in HTP, while the MCT
668 simulation exhibits lower CO total columns and clear underestimation in the Beijing region. This is also
669 consistent with results of the comparison of CO emissions displayed on Table 2, which indicate CO
670 amounts in Beijing in MACCity lower by 78% compared to HTAPv2.

671 Comparison of the predicted monthly mean NO₂ tropospheric columns with GOME2 observations are
672 displayed on Figure 9. For a proper comparison, simulated NO₂ distributions are transformed using the
673 GOME2 averaging kernels following Eskes and Boersma (2003). Due to the short NO₂ lifetime, its
674 high concentrations are generally correlated with high emissions areas, which are mostly located in the
675 north-eastern regions such as Beijing but also in the Shanghai and Guangzhou regions and in the
676 Sichuan basin. Overall, the spatial patterns of tropospheric NO₂ columns in January 2010 are
677 reproduced reasonably by all the simulations. The NO₂ values in the north-eastern regions are however
678 better captured by HTP compared in particular to the MCT simulation. This is consistent with the
679 results discussed in Sect. 5.1, which show a better agreement of HTP with surface NO_x measurements
680 in the Beijing region in January 2010 compared to other simulations (see also Figure 10). All the
681 simulations underestimate NO₂ tropospheric columns in the Guangzhou region, consistent also with the
682 results discussed in Sect. 5.1 (see also Figure 13), but show overestimations in the Sichuan basin.
683 GOME2 observations for July 2010 show a broader region of high NO₂ tropospheric columns in north

684 eastern China compared to the model predictions. HTP shows slightly better agreement with GOM2 ,
685 while MCT shows much lower concentrations and higher underestimation, which is linked to the lower
686 NO emissions in MACCity (Table2).

687 The discrepancies found between the simulations and MOPITT and GOME2 observations should not
688 completely incriminate the model performance or the emissions used. It could also be due to
689 uncertainties in satellite retrievals. For example, previous studies have shown that significant
690 uncertainties in NO₂ satellite observations could result from the different assumptions used in the
691 retrievals calculations, such as the cloud mask applied, airmass factors, the stratosphere-troposphere
692 separation, and system errors due to surface reflectivity and aerosols (Richter and Burrows, 2002;
693 Martin et al., 2002; Boersma et al. 2004). The relative errors can reach 40-60% in polluted areas of
694 China (Ma et al, 2006; Boersma et al. 2004), indicating that careful interpretation is required in
695 quantitative model evaluation with satellite measurements.

696

697 **5. Evaluation against surface measurements**

698 **5.1 Evaluation with surface observations in January 2010**

699 Figure 10 illustrates time series of simulated and observed surface concentrations of NO_x, O₃, CO, SO₂,
700 PM_{2.5} and PM₁₀ in Beijing in January 2010. The three model simulations HTP, RAS and MCT replicate
701 correctly the variability of all observed species and capture the increase of concentrations during two
702 pollution episodes that occurred during the second and third week of January 2010. The statistical
703 indicators displayed in Table 3 confirm the good agreement between all the simulations and the
704 observations, with IOA and R values higher than 0.5 and 0.6, respectively, for most of the species. The
705 simulations meet also the performance goals for particulates (MFB and MFE limits of ± 0.3 and 0.5,
706 respectively) as recommended by Boylan and Russel (2006). The HTP simulation captures however
707 better than RAS and MCT the peak concentrations of NO_x and particulates during the two pollution
708 events in January 2010. In terms of bias, HTP produces also lower MB and MFB values for NO_x, SO₂
709 and PM₁₀, while MCT exhibits higher biases in general compared to the two other simulations. Low O₃
710 concentrations are observed in Beijing in January and the model simulations exhibit comparable
711 performances with small MB and MFB, good correlation (R>0.6) and a good index of agreement
712 (IOA>0.52). All model simulations tend to underestimate CO concentrations in the unique CO
713 measurement site in Beijing. The peak CO concentrations observed during the two pollution episodes in

714 January (3.5 and 6 ppm respectively) are underpredicted by more than 50% with the highest bias found
 715 in MCT due most likely to lower CO anthropogenic emissions in the MACCity inventory as discussed
 716 in Section 4.1.

717 Table 3: Statistical skills in Beijing, Shanghai and Guangzhou in January 2010 with the HTP
 718 (left columns), RAS (center columns) and MCT (right columns) model simulations.
 719

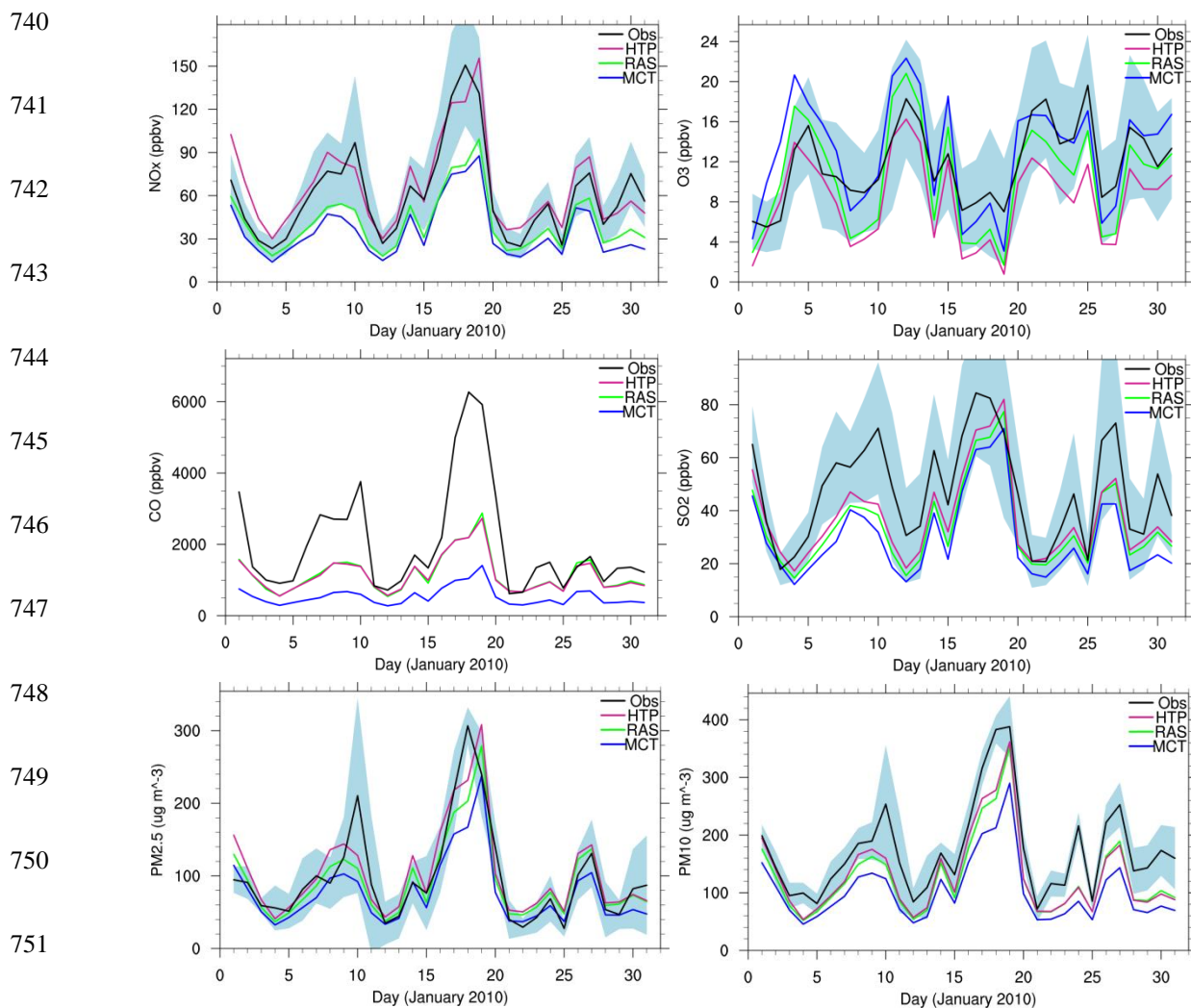
Beijing	NOx			O₃			SO₂			PM_{2.5}			PM₁₀		
MB	6.3	-19.4	-25.3	-3.7	-1.5	1.1	-9.5	-13.2	-17.6	17.1	0.11	-12.6	-31.1	-35.5	-61.9
MFB	0.10	-0.25	-0.45	-0.49	-0.16	0.04	-0.21	-0.28	-0.38	0.28	0.17	0.04	-0.23	-0.24	-0.44
MFE	0.44	0.58	0.70	0.67	0.50	0.55	0.57	0.52	0.64	0.51	0.43	0.45	0.43	0.41	0.52
RMSE	44.8	41.1	44.8	6.96	6.61	8.22	31.1	28.6	34.8	72.1	64.8	70.1	84.7	80.4	97.1
R	0.60	0.65	0.63	0.75	0.70	0.59	0.59	0.70	0.54	0.69	0.72	0.67	0.68	0.72	0.67
IOA	0.52	0.58	0.53	0.60	0.63	0.52	0.59	0.63	0.55	0.64	0.72	0.71	0.61	0.62	0.54

Shanghai	NOx			O₃			PM_{2.5}			PM₁₀		
MB	31.6	64.1	-19.8	-5.3	-6.8	2.4	1.5	5.1	4.4	-4.8	13.7	-2.1
MFB	0.26	0.57	-0.51	-0.68	-1.0	0.14	-0.08	-0.07	-0.03	-0.13	0.03	-0.09
MFE	0.54	0.65	0.65	0.73	1.0	0.74	0.32	0.37	0.33	0.34	0.33	0.33
RMSE	63.5	98.9	35.5	9.18	10.3	8.38	32.0	41.8	35.1	42.1	61.7	44.8
R	0.60	0.50	0.59	0.65	0.62	0.68	0.79	0.76	0.77	0.75	0.73	0.74
IOA	0.14	-0.26	0.45	0.61	0.56	0.63	0.63	0.55	0.61	0.63	0.54	0.62

Guangzhou	NO₂			O₃			SO₂			PM_{2.5}			PM₁₀		
MB	-4.3	-6.3	-4.4	-14.4	-10.7	-8.4	6.6	0.8	7.4	17.2	22.8	37.1	-0.8	10.5	21.6
MFB	-0.11	-0.19	-0.12	-0.63	-0.32	-0.20	0.29	0.11	0.33	0.34	0.42	0.60	0.10	0.20	0.29
MFE	0.47	0.45	0.48	0.65	0.47	0.42	0.33	0.22	0.36	0.51	0.52	0.61	0.53	0.53	0.54
RMSE	19.7	18.3	19.7	19.3	17.1	15.7	13.2	4.9	9.7	35.6	38.8	48.6	54.5	55.3	55.5
R	0.51	0.66	0.64	0.36	0.37	0.30	0.48	0.68	0.51	-0.06	-0.09	0.08	-0.09	-0.02	-0.01
IOA	0.45	0.47	0.46	0.48	0.52	0.50	0.22	0.51	0.28	0.23	0.16	-0.08	0.41	0.39	0.36

722
 723
 724 We present in this section an analysis of the major pollution episode that occurred on 15-20 January in
 725 north-eastern China. As displayed on Figure 10, NO_x, CO, SO₂, PM_{2.5} and PM₁₀ concentrations reached
 726 the extremely high values of 150 ppb, 6 ppm, 80 ppb, 300 μg m⁻³ and 400 μg m⁻³, respectively on 18
 727 January 2010. During this pollution episode, the wind speed measurements in Beijing (see Figure 2)
 728 decreased to less than 1 m s⁻¹ indicating air stagnation and thus accumulation of pollutants in the lower
 729 troposphere. Analysis of the modeled vertical distribution of temperature (Figure 11) shows a positive
 730 gradient in the layer 200 m to 1.4 km and an inversion layer below 200 m. Such conditions reduce the
 731 vertical mixing and lead to the build-up of primary pollutants in the boundary layer. The relative

732 humidity increased to up to 70% during this pollution episode (see Figure 2). This moist atmosphere
 733 situation may have led also to the formation of secondary pollutants. The increase in NO_x
 734 concentrations combined with high aerosol loading, which can decrease the photochemical activity due
 735 to low radiation, could explain the observed high ozone loss during this pollution event. As discussed in
 736 Section 3, the model reproduces relatively well the meteorological situation in Beijing in January 2010.
 737 This explains the good performance of the model simulations during this particular pollution event. The
 738 moderate pollution event that occurred in the second week of January could also be due to stable
 739 meteorological situation with low wind speed values as indicated on Figure 2.



752 Figure 10: Time series of observed and simulated daily mean concentrations of NO_x,
 753 O₃, CO, SO₂, PM_{2.5} and PM₁₀ in Beijing for January 2010. Standard deviations from
 the mean observations indicated with shaded area.

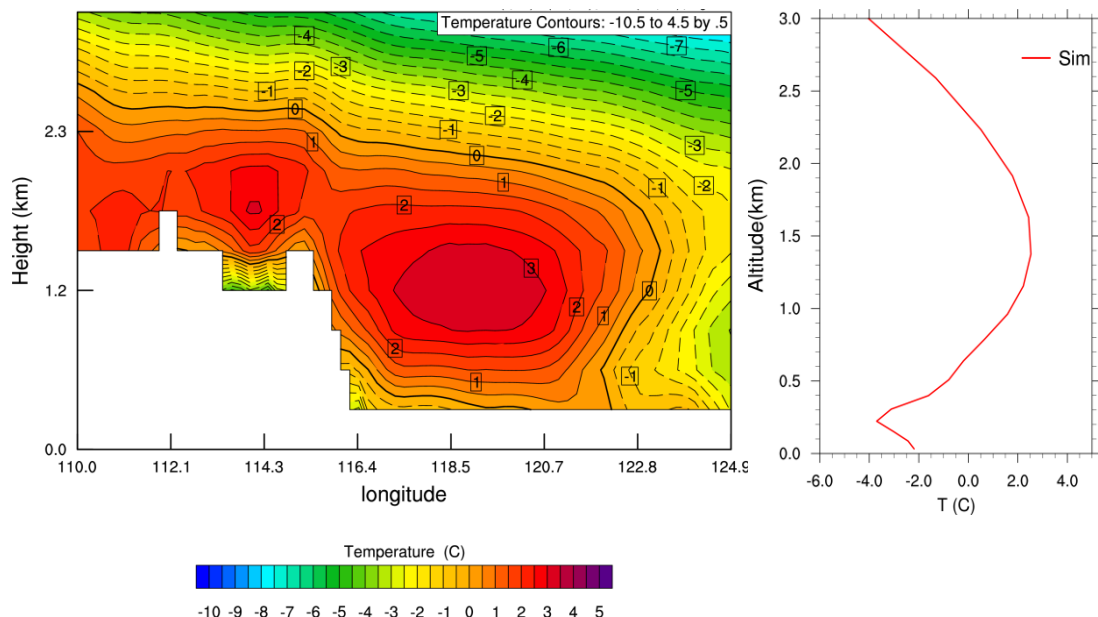


Figure 11: Vertical cross-section of simulated temperature (°C) at 39.91°N (left) and vertical profile of temperature (up to 3 km altitude) in Beijing on 18 January 2010 (right).

Comparison of the model predictions with surface measurements in Shanghai in January 2010 are displayed on Figure 12. The Shanghai region did not experience a particular haze event similar to the one observed in Beijing, but high NO_x , $\text{PM}_{2.5}$ and PM_{10} concentrations of over 80 ppb, $150 \mu\text{g m}^{-3}$ and $180 \mu\text{g m}^{-3}$ respectively were also observed in this region in January 2010. The three WRF-Chem simulations reproduce well the concentrations and temporal variability of $\text{PM}_{2.5}$ and PM_{10} . They exhibit almost similar statistical performances (Table 3) and good agreement with the measurements ($R > 0.73$ and $\text{IOA} > 0.54$). We can notice in particular the low MB, MFB and MFE values which meet well the performance goals suggested by Boylan and Russel (2006). The simulations show also good correlation with the observations and reproduce well the temporal variability of NO_x and O_3 (R higher than 0.5 and 0.62, respectively). They exhibit however significant differences in the predicted NO_x and O_3 concentrations. The RAS and HTP simulations tend to overestimate NO_x as indicated by the high MB, MFB and MFE values in Table 3, and show low agreement indices (IOA of -0.26 and 0.14, respectively). The MCT simulation shows a better index of agreement with NO_x measurements ($\text{IOA} = 0.45$) but tend to underestimate the NO_x concentrations ($\text{MB} = -19.8$). In general, predicted NO_x and O_3

778 in Shanghai are anti-correlated, and this could explain the systematic lower O₃ in RAS and HTP (MFB
 779 of -1 and -0.68 respectively) and the better performance of MCT (MB = 2.4, MFB = 0.14). The
 780 differences between the simulations regarding the predicted NO_x and O₃ could be driven by the
 781 differences in the emissions and their resolution. The high resolution characterizing the HTAPv2 and
 782 REASv2 emissions, used in HTP and RAS simulations respectively, better resolves the emission
 783 sources, particularly in Shanghai which is close to the ocean, while the MACCity emissions used in
 784 MCT are more representative of large areas. Furthermore, as shown on Table 1, NO emissions in
 785 Shanghai are higher by more than 30% in HTAPv2 and REASv2 inventories compared to MACCity.

786

787

788

789

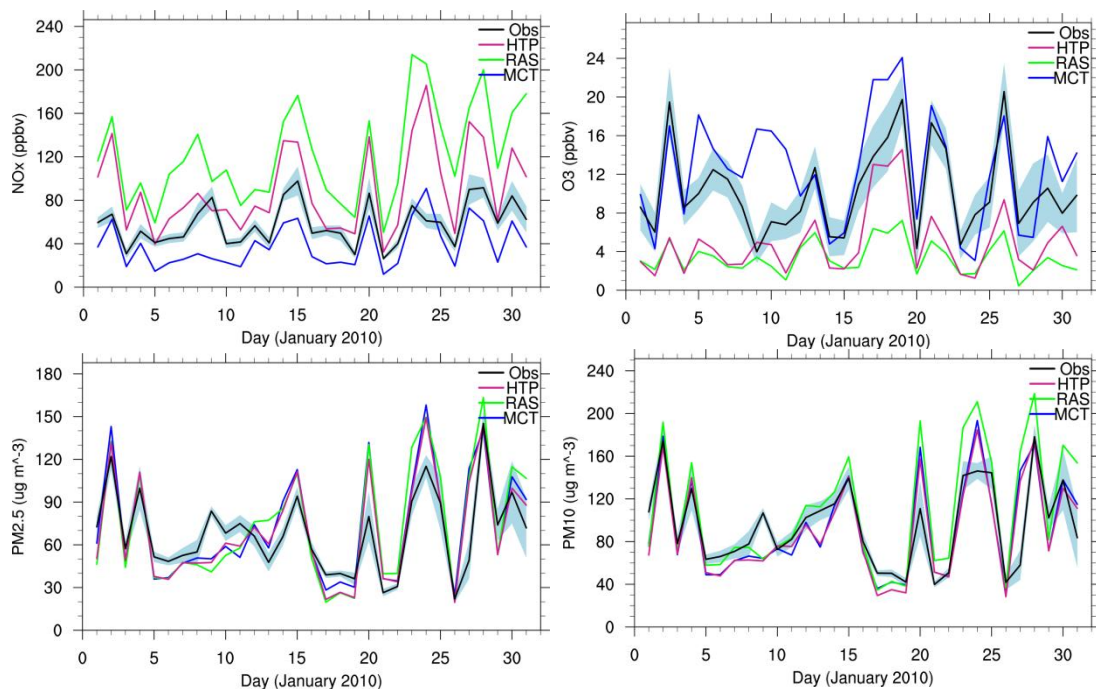
790

791

792

793

794



795 Figure 12: Time series of simulated and observed daily mean NO_x, O₃, PM_{2.5} and PM₁₀
 796 concentrations in Shanghai in January 2010. Standard deviations from the mean
 797 observations indicated with shaded area.

797

798

799

800

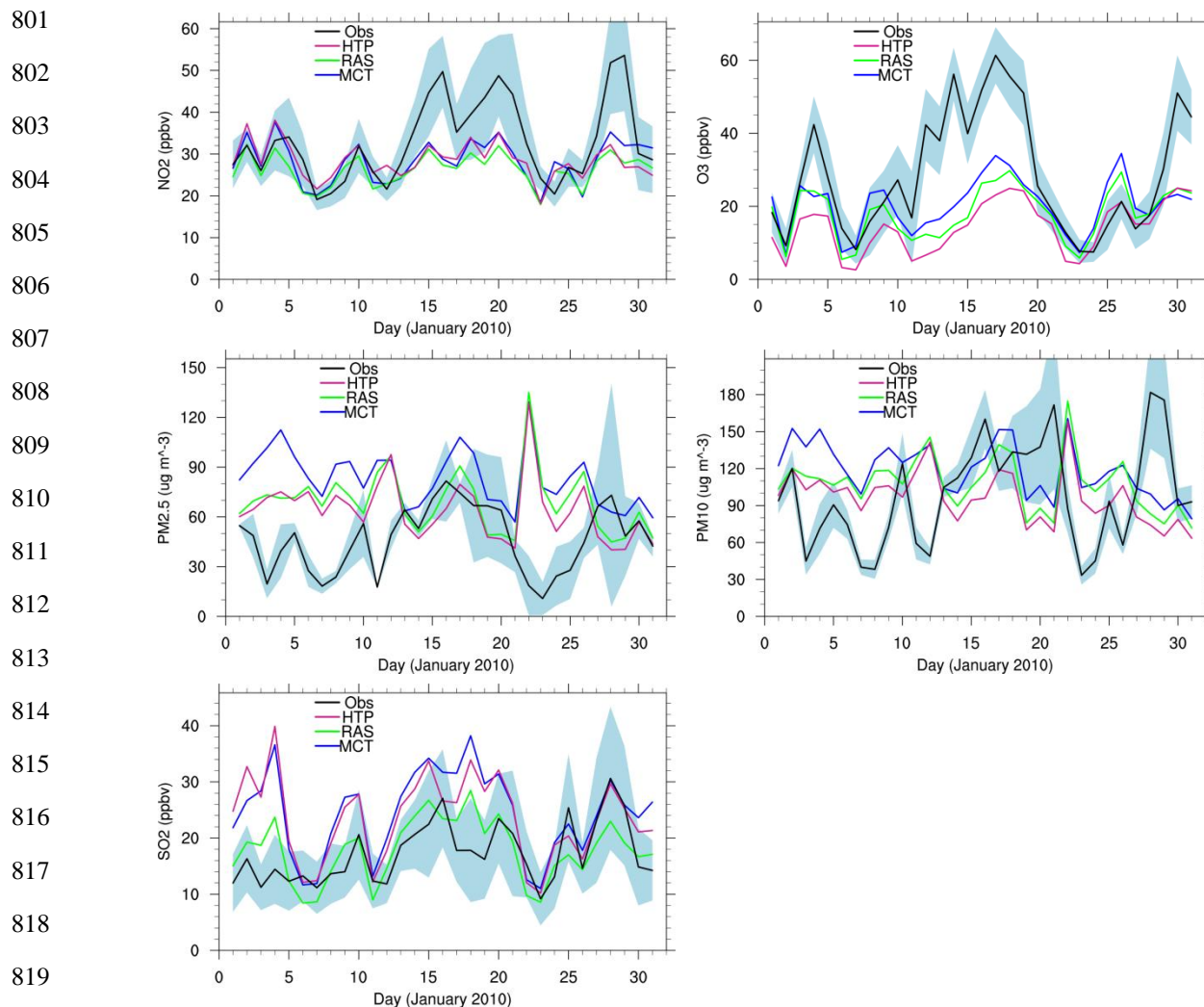


Figure 13: Time series of simulated and observed daily mean NO_2 , O_3 , $\text{PM}_{2.5}$, PM_{10} and SO_2 concentrations in Guangzhou for January 2010. Standard deviations from the mean observations indicated with shaded area.

The model results and statistical measures in Guangzhou in January 2010 are illustrated on Figure 13 and Table 3, respectively. The simulations produce generally good agreement indices for NO_2 and O_3 ($\text{IOA} > 0.45$) and comparable statistical measures but tend to underestimate the O_3 and NO_2 concentrations in mid- and end of January 2010. This is consistent with the statistical indicators on Table 3, which show negative MB and MFB. There are almost no differences in the predicted NO_2 concentrations between the simulations and only slight differences (~ 5 ppb) are found for O_3 . This suggests that other processes than emissions are responsible for the underestimation of surface O_3 and

830 NO₂ in the simulations. The meteorological situation in Guangzhou (Figure 4) is characterized by a
831 decrease in wind speed to less than 2 m s⁻¹ in mid- and end of January. This leads to unfavourable
832 conditions for the dispersion of pollution and could explain the observed high NO₂ concentrations (40-
833 50 ppb). The temperature increased to around 20 °C in mid-January, while relative humidity showed the
834 lowest observed values in January 2010. The observed O₃ increases could partially be related to the
835 combination of high temperature and low humidity, which can increase the O₃ formation rates. While
836 the temperature profile is well predicted by the model, the relative humidity is slightly overestimated
837 and this may have led to a lower O₃ production rate in the model. Uncertainties in VOC emissions in the
838 inventories combined with the underestimation of NO₂ could also result in less efficient O₃ formation in
839 the model. For SO₂, the RAS simulation exhibits better agreement with the observations (IOA = 0.51)
840 and higher scores (e.g. MB = 0.8, MFE = 0.22 and R = 0.68) compared to HTP and MCT simulations,
841 which tend to overestimate SO₂. The model simulations fail to reproduce correctly the temporal
842 variability of PM_{2.5} and PM₁₀ in Guangzhou in January 2010. Although the simulations achieve the
843 model performance criteria for particulates (MFE ≤ +0.75% and MFB ≤ ±0.6) proposed by Boylan and
844 Russel (2006), they fail to meet the strict performance goals (MFE ≤ +0.5 and MFB ≤ ±0.3). As
845 indicated on Figure 4, the precipitation rates in Guangzhou are underestimated in the model in
846 beginning and end of January 2010. This may have led to less removal of aerosols by wet scavenging in
847 the model and could explain the discrepancies between the simulated and observed PM_{2.5} and PM₁₀.
848 Overall, the results indicate that meteorological conditions have also important impact on the
849 concentrations of pollutants in Guangzhou. Further investigations on e.g. aerosol formation,
850 composition and properties in the Guangzhou region, and on the role of land-sea interaction processes,
851 regional topography and vertical mixing could help better understand the discrepancies between the
852 model and the observations.

853

854 **5.2 Evaluation with surface observations in July 2010**

855 The observed O₃ concentrations in Beijing in July 2010 show maximum values of ~50 ppb (Figure 14),
856 which are higher than that in January 2010 (~25 ppb) due to high photochemical activity in summer. On
857 the other hand, maximum NO_x concentrations in July 2010 (~35 ppb) correspond to the minimum
858 values observed in Beijing in January 2010. Clear differences can be seen between the three model
859 simulations for most of the pollutants. The HTP simulation shows NO_x values between 30 and 45 ppb,

860 which are nearly two times higher than what RAS and MCT have predicted (15-20 ppb). This is in
861 agreement with the differences in NO emissions in Beijing in July, discussed in Sect. 4.1 (see also Table
862 2), which are higher in HTAPv2 than in MACCity and REASv2. The HTP results indicate overestimate
863 of NO_x (MB=9.3 and MFB=0.23 on Table 4) while the RAS and MCT simulations show an
864 underestimations with NO_x concentrations lower by 10 to 20 ppb compared to the observations (e.g.
865 MB = -9.9 and RMSE = 15.4 for RAS). All the simulations show moderate agreement indices (IOA <
866 0.36) and correlation coefficients (R<0.39) due to the temporal variability of NO_x observations, which
867 is not well captured by the simulations. In relation to the underestimation of NO_x concentrations, the
868 MCT and RAS results show higher positive O₃ biases (e.g. MFB and MFE >0.5) while HTP exhibits
869 better agreement (IOA=0.37) and correlation with the observations (R=0.51) and lower bias (MB=12.6
870 and MFB=0.29).

871 Table 4: Statistical skills in Beijing, Shanghai and Guangzhou in July 2010 with the HTP (left
872 columns), RAS (center columns) and MCT (right columns) model simulations.

Beijing	NO _x			O ₃			SO ₂			PM _{2.5}			PM ₁₀		
MB	9.3	-9.9	-12.8	12.6	31.7	23.7	16.5	13.2	8.2	26.2	28.4	10.7	-6.9	3.9	-23.1
MFB	0.23	-0.46	-0.68	0.29	0.61	0.50	1.24	1.22	0.99	0.32	0.35	0.18	-0.03	0.05	-0.16
MFE	0.47	0.59	0.77	0.40	0.62	0.53	1.24	1.22	1.01	0.44	0.43	0.37	0.35	0.32	0.35
RMSE	23.6	15.4	18.1	21.7	36.7	29.9	20.6	14.5	9.8	46.9	43.8	35.2	55.7	51.4	55.9
R	0.39	0.25	0.04	0.51	0.37	0.31	0.23	0.44	0.39	0.48	0.61	0.58	0.46	0.56	0.50
IOA	0.14	0.36	0.23	0.37	-0.14	0.07	-0.65	-0.56	-0.32	0.41	0.44	0.55	0.47	0.51	0.48

Shanghai	NO _x			O ₃			PM _{2.5}			PM ₁₀		
MB	29.6	61.1	-3.6	2.3	-1.9	16.7	35.1	44.2	33.6	43.3	66.3	41.1
MFB	0.75	1.08	-0.09	-0.16	-0.24	0.47	0.75	0.85	0.76	0.70	0.90	0.69
MFE	0.74	1.08	0.62	0.30	0.41	0.49	0.78	0.87	0.79	0.73	0.92	0.74
RMSE	35.4	65.6	15.7	21.6	24.3	27.6	51.7	65.2	48.6	64.3	82.4	52.1
R	0.49	0.47	0.33	0.69	0.71	0.67	0.64	0.60	0.63	0.59	0.53	0.59
IOA	-0.28	-0.63	0.64	0.61	0.56	0.46	-0.22	-0.38	-0.19	-0.28	-0.51	-0.23

Guangzhou	NO ₂			O ₃			SO ₂			PM _{2.5}			PM ₁₀		
MB	3.3	0.3	0.6	-25.3	-21.8	-22.1	12.4	4.3	6.6	4.4	2.1	8.7	-0.2	-2.1	4.5
MFB	0.20	0.07	0.07	-0.78	-0.64	-0.65	0.80	0.42	0.64	0.22	0.13	0.35	-0.01	-0.07	0.11
MFE	0.47	0.45	0.49	0.80	0.68	0.69	1.06	0.76	0.84	0.37	0.43	0.45	0.44	0.46	0.49
RMSE	9.9	8.4	9.1	32.2	28.8	29.1	18.9	9.80	11.6	10.2	12.1	14.7	22.9	21.7	25.5
R	0.45	0.44	0.48	0.46	0.54	0.53	-0.06	0.05	-0.18	0.63	0.57	0.54	0.64	0.63	0.57
IOA	0.38	0.46	0.41	0.28	0.36	0.35	-0.49	0.03	-0.15	0.52	0.46	0.33	0.44	0.46	0.35

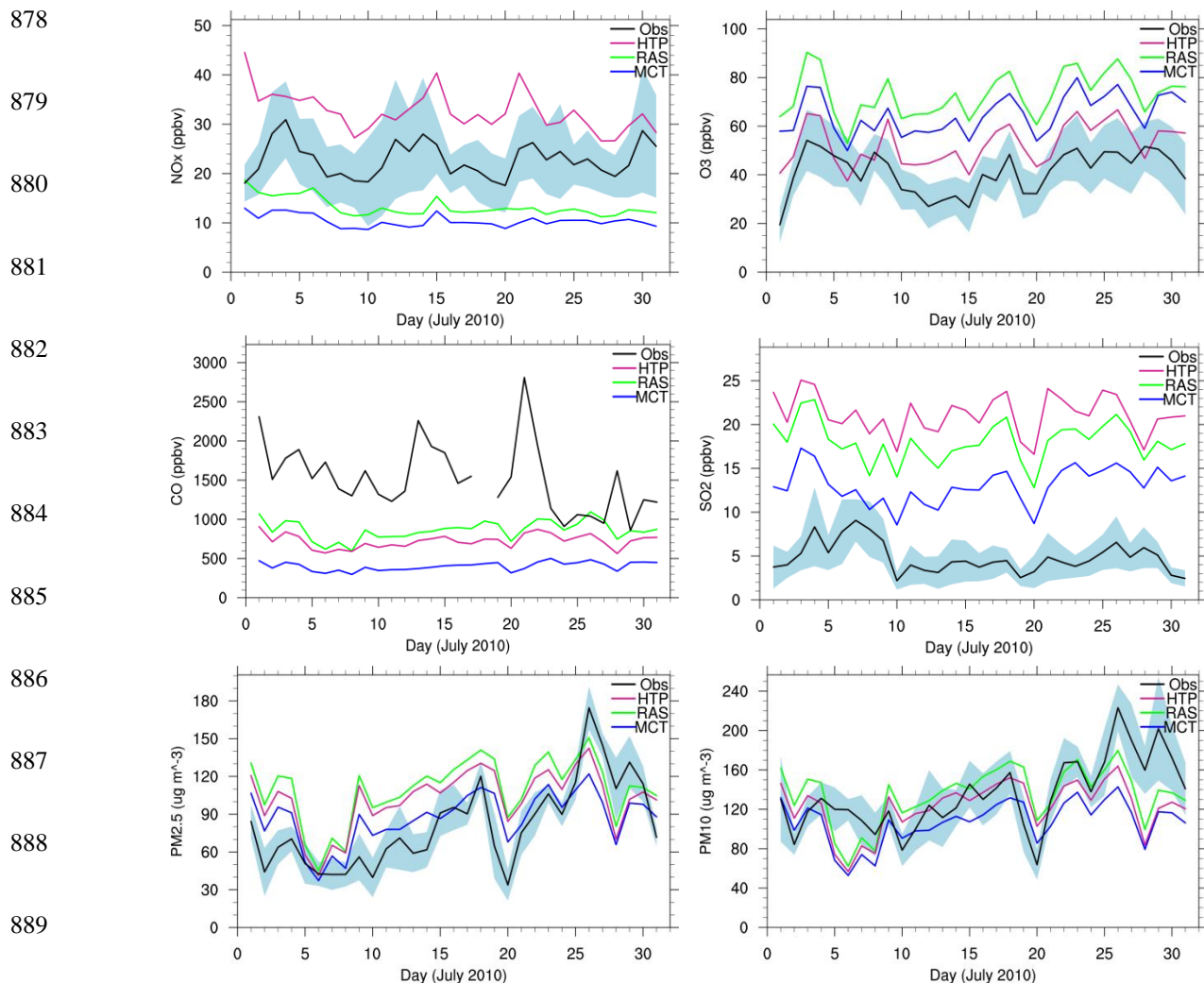
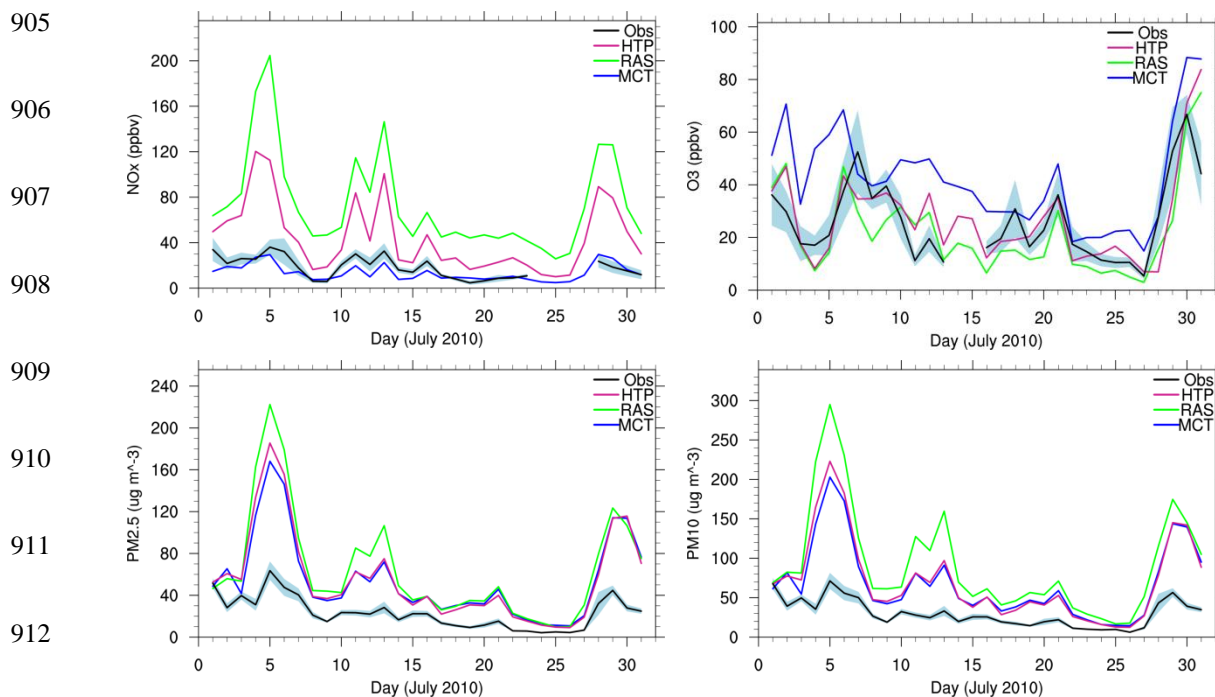


Figure 14: Time series of simulated and observed daily mean concentrations of NO_x, O₃, CO, SO₂, PM_{2.5} and PM₁₀ in Beijing in July 2010. Standard deviations from the mean observations indicated with shaded area.

As in January, all the simulations underestimate CO concentrations in July 2010 and fail to capture correctly the observed peak concentrations at the CO measurement site in Beijing. The HTP and RAS simulations predicted CO concentrations (~1 ppm) lower by 0.5 to 1 ppm compared to the observations, while MCT predicted the lowest CO concentrations (~0.5 ppm) due to lower CO emissions and resolution in the MACCity inventory. For SO₂, we can notice the lower concentrations in July (<10 ppb) compared to observed values in January 2010 (up to 85 ppb). All the three simulations show overestimation of SO₂ by more than of factor of two indicating possible overestimation of SO₂

900 emissions in summer in the emission inventories. The three simulations reproduce correctly the
 901 temporal variability of $PM_{2.5}$ and PM_{10} concentrations including the abrupt decreases on 20 July and
 902 increases at the end of July. The simulations meet also the performance goal for particulates. Their
 903 statistical scores are generally comparable and indicate good agreement ($IOA > 0.41$) with the
 904 observations (Table 4).



913 Figure 15: Time series of simulated and observed daily mean NO_x , O_3 , $PM_{2.5}$ and
 914 PM_{10} concentrations in Shanghai in July 2010. Standard deviations from the mean
 915 observations indicated with shaded area.

916 The model results for Shanghai in July 2010 (Figure 15) indicate that the MCT simulation captures well
 917 the NO_x observations, with low bias ($MB = -3.6$, $MFB = -0.09$, see Table 4) and good index of
 918 agreement ($IOA = 0.64$). The HTP and RAS simulations overpredict the NO_x concentrations (MFB of
 919 0.75 and 1.08 respectively) and show abrupt and high increases of NO_x during the first, second and last
 920 weeks of July 2010, which are not seen in the observations. This explains the lower statistical skills and
 921 lower agreement of HTP and RAS with the NO_x measurements. Despite the good performance of the
 922 MCT simulation for NO_x , it shows however lower statistical skills for O_3 and higher bias ($MFB = 0.47$,

923 MFE = 0.49) compared to HTP and RAS, which agree better with the observations (e.g. IOA=0.61 and
924 MB=2.3 for HTP).

925 The results for PM_{2.5} and PM₁₀ in Shanghai indicate overestimations in all the simulations and abrupt
926 increases which coincide to the time periods of maximum overestimations of NO_x in HTP and RAS
927 simulations. The performance goals and criteria for particulates are therefore not achieved (MFB >0.69,
928 MFE >0.74) and the agreement indices are low and negative. The temporal variability is however
929 relatively well captured by the simulations which show relatively good correlation coefficients.
930 Analysis of model prediction of wind speed in Shanghai in July (Sect. 3, see also Figure 3) shows that
931 while wind speed is generally overestimated in the model, rapid decreases with values almost lower
932 than the observations, have occurred during the same time periods of overestimations of PM_{2.5} and PM₁₀
933 and NO_x concentrations. Such rapid decreases in wind speed and close proximity to emissions sources
934 in particular in HTAPv2 and RASv2 emissions, could have led to strong accumulation of pollution in
935 the model and thus to the overestimations of PM_{2.5} and PM₁₀ and NO_x.

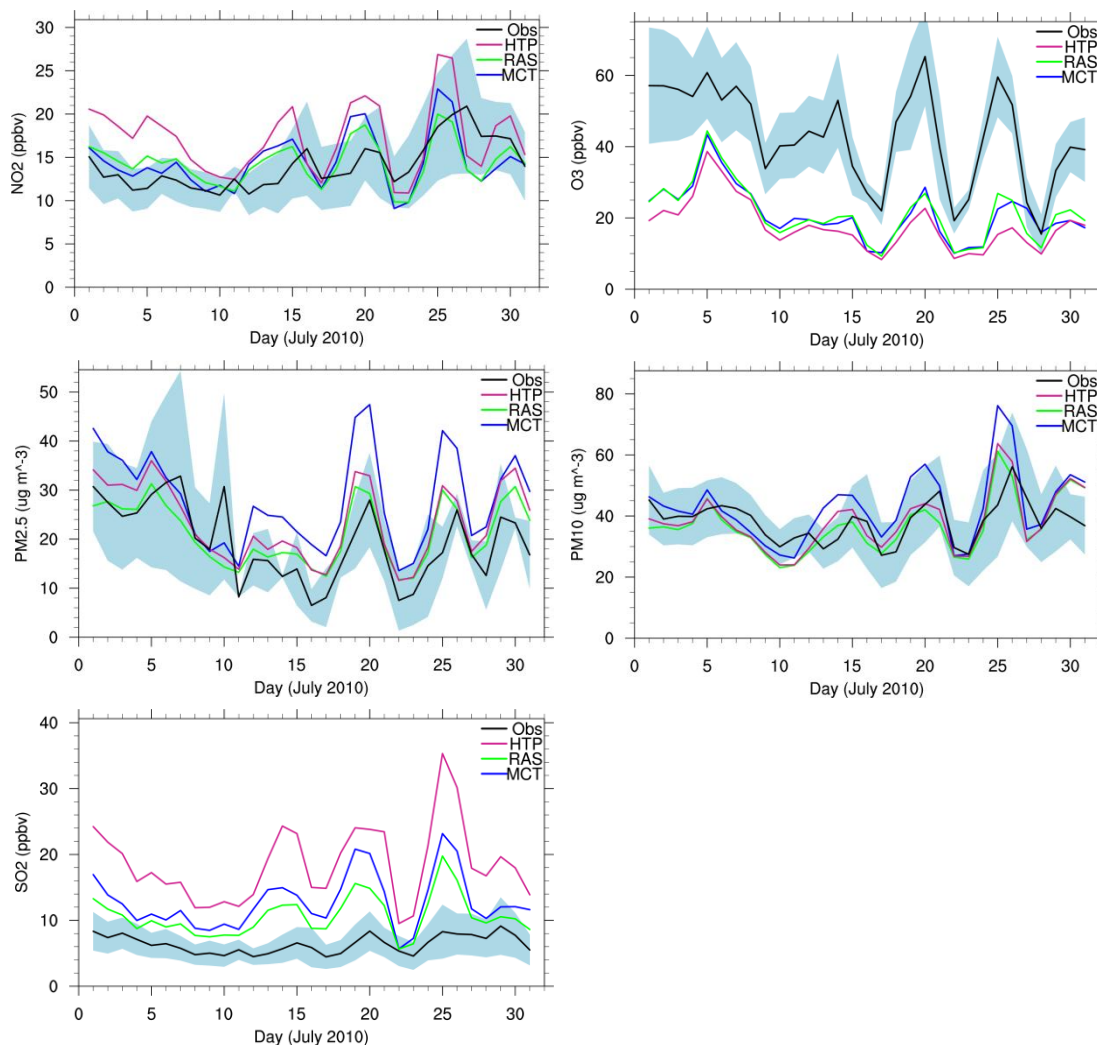
936

937 Figure 16 illustrates the model results in Guangzhou in July 2010. The three model simulations show
938 almost similar O₃ profiles and capture relatively well the temporal variability of O₃ but tend to
939 underestimate the observed concentrations by more than 30 ppb, consistent with the statistical scores on
940 Table 4 (negative MB and MFB values). The observed NO₂ concentrations are well captured by the
941 three simulations, although HTP tends to show an overestimation (MFB = 0.20) and a slightly lower
942 agreement (IOA = 0.38) with the measurements compared to RAS and MCT (IOA = 0.46 and 0.41,
943 respectively). Observed SO₂ concentrations in Guangzhou remained below 10 ppb in July 2010 while
944 the simulations showed higher values. In particular, HTP predicted SO₂ concentrations higher by more
945 than two times (MB = 12.4, RMSE = 18.9). This was also noticed in Beijing in July and suggests
946 overestimation of SO₂ emissions in summer in the three emission inventories. The observed PM_{2.5} and
947 PM₁₀ concentrations and temporal variability are nicely captured by the HTP and RAS simulations,
948 which meet the strict performance goals for particulates suggested by Boylan and Russel (2006). The
949 MCT simulation shows also good skills (Table 4) and meet the performance criteria for particulates,
950 although it overestimates slightly the PM_{2.5} concentrations (MFB = 0.35, MFE=0.45).

951

952

953
954
955
956
957
958
959
960
961
962
963
964
965
966
967
968
969
970
971



972 Figure 16: Time series of simulated and observed daily mean NO_2 , O_3 , $\text{PM}_{2.5}$ and
973 PM_{10} concentrations in Guangzhou for July 2010. Standard deviations from the mean
974 observations indicated with shaded area.

975

976 6. Conclusions

977 The online coupled model WRF-Chem was used to investigate the air quality characteristics in eastern
978 China and to assess the model performance in January and July 2010. The evaluation of the modelling
979 system was performed using both satellite and ground-based measurements and was conducted
980 specifically for the highly populated and polluted regions of Beijing, Shanghai and Guangzhou. Model
981 simulations were performed using the HTAPv2, REASv2 and MACCity anthropogenic emission
982 inventories to assess the impact of emissions on the model predictions.

983 Overall, the selected WRF-Chem configuration shows satisfactory results and captures generally well
984 the distributions of major air pollutants in eastern China in both summer and winter conditions. In
985 particular, the defined goals for the concentrations of particulates are met by the model simulations in
986 most of the considered regions. The simulated meteorological fields agree also generally well with the
987 observations in general in the three selected city-clusters, but the model tends to overestimate the
988 maximum values of surface wind speed, as also reported in previous WRF-Chem modelling studies.
989 The ability of the model to capture specific pollution events under specific meteorological conditions is
990 demonstrated with the good performance and statistical skills of the simulations during the pollution
991 event that was observed in Beijing in mid-January 2010. This event led to high concentrations of NO_x
992 (150 ppb) CO (6 ppm), SO₂ (80 ppb) PM_{2.5} (300 µg m⁻³) and PM₁₀ (400 µg m⁻³) and is found to be
993 related to temperature inversion in the lower troposphere, which resulted in a stagnation situation and
994 build-up of air pollution. The HTAPv2-based simulation showed generally better agreement with the
995 observations during this event compared to results of the REASv2-based and MACCity-based
996 simulations.

997 This study highlights the extent of uncertainties in actual inventories of anthropogenic emissions for
998 China. The HTAPv2, REASv2 and MACCity anthropogenic emissions show differences in magnitude
999 ranging from less than 10% to more than 80% for some species (e.g. NO and CO) and indicate also
1000 differences in the temporal and spatial distribution of the emissions. As a result, large differences in the
1001 predicted concentrations of major pollutants are found between the WRF-Chem simulations conducted
1002 separately using these emission inventories. For instance, the HTAPv2- and REASv2-based simulations
1003 better reproduce the magnitude and spatial distribution of CO total columns and NO₂ tropospheric
1004 columns derived from MOPITTv6 and GOME2 satellite observations respectively. On the other hand,
1005 the MACCity-based simulation tends to produce lower CO and NO₂ concentrations, and lower
1006 performance when compared to satellite observations. The model simulations exhibit also clear
1007 differences, in particular in Shanghai and Beijing in January and July 2010 respectively, which can be
1008 linked to the differences in the emissions.

1009 This study highlights however that the discrepancies between the model and the observations cannot
1010 always be attributed to uncertainties and differences in the emission estimates. Regardless of the
1011 emissions applied, the model failed to correctly capture the concentrations and temporal variability of

1012 air pollutants in some particular cases. For example, inaccuracies in the predicted meteorological
1013 parameters, such as precipitation rates in Guangzhou in January 2010 and wind speed in Shanghai in
1014 July 2010, resulted in lower performance and statistical skills in all the simulations. Improved model
1015 resolution and better understanding of the processes affecting aerosol formation, composition and
1016 properties and atmospheric composition in general in some regions like Guangzhou are therefore
1017 required. Correct prediction of the meteorological fields is also key for a reliable air quality prediction
1018 particularly during pollution events. Further investigations on the role of land-sea interaction processes,
1019 regional topography and vertical mixing could also help better understand the discrepancies between the
1020 model and the observations. Overall, this study provided an opportunity to assess the performance of the
1021 selected WRF-Chem model settings, and led to the implementation of the model as an operational
1022 forecasting system for regional air quality in China.

1023

1024 ***Acknowledgements***

1025 This work has received research funding from the European Community's Seventh Framework
1026 Programme (FP7) under the PANDA project grant agreement n° 606719. This work was also partially
1027 supported by the National Key Research and Development Program of China (2017YFC0210105),
1028 National Natural Science Funds of China (No.41425020).

1029 The authors gratefully acknowledge the computing time granted by the John von Neumann Institute for
1030 Computing (NIC) and provided on the supercomputer JURECA at the Jülich Supercomputing Centre
1031 (JSC). We acknowledge use of MOZART-4 global model output available at
1032 <http://www.acom.ucar.edu/wrf-chem/mozart.shtml>. We acknowledge also use of the WRF-Chem
1033 preprocessor tool {mozbc, fire_emiss, etc.} provided by the Atmospheric Chemistry Observations and
1034 Modelling Lab (ACOM) of NCAR.

1035

1036 **References**

1037

1038 Akimoto, H., Global air quality and pollution, *Science*, 302(5651):1716-9, 2003.

1039

1040 Amnuaylojaroen, T., Barth, M. C., Emmons, L. K., Carmichael, G. R., Kreasuwun, J.,
1041 Prasitwattanaseree, S., and Chantara, S.: Effect of different emission inventories on modeled ozone and
1042 carbon monoxide in Southeast Asia, *Atmos. Chem. Phys.*, 14, 12983-13012, doi:10.5194/acp-14-12983-
1043 2014, 2014.

1044

1045 Ashmore, M. R.: Assessing the future global impacts of ozone on vegetation. *Plant, Cell &*
1046 *Environment*, 28: 949–964. doi:10.1111/j.1365-3040.2005.01341.x, 2005.

1047

1048 Boersma, K. F., and Eskes, H., Assimilated SCIAMACHY NO₂ fields, HDF data file user manual,
1049 (http://www.temis.nl/airpollution/no2col/papers/no2col_hdf_docu.pdf, last accessed 15.02.2018), 2004.
1050

1051 Boersma, K. F., Eskes, H. J., and Brinksma, E. J.: Error analysis for tropospheric NO₂ retrieval from
1052 space, *J. Geophys. Res.*, 109, D04311, doi:10.1029/2003JD003962, 2004.
1053

1054 Boersma, K. F., Eskes, H. J., Veefkind, J. P., Brinksma, E. J., van der A, R. J., Sneep, M., van den
1055 Oord, G. H. J., Levelt, P. F., Stammes, P., Gleason, J. F., and Bucsela, E. J.: Near-real time retrieval of
1056 tropospheric NO₂ from OMI, *Atmos. Chem. Phys.*, 7, 2103–2118, doi:10.5194/acp-7-2103-2007, 2007.
1057

1058 Bouarar, I., X. Wang and Brasseur, G. P. (Eds.), *Air Pollution in Asia: An Integrated Perspective*,
1059 Springer, ISBN 978-3-319-59489-7, 2017.
1060

1061 Boylan, J. W., and A. G. Russell, PM and light extinction model performance metrics, goals, and
1062 criteria for three-dimensional air quality models. *Atm. Env.*, 40:4946–4959, 2006.
1063

1064 Boynard, A., Clerbaux, C., Clarisse, L., Safieddine, S., Pommier, M., Van Damme, M., Bauduin, S.,
1065 Oudot, C., Hadji-Lazaro, J., Hurtmans, D., Coheur, P.-F, First simultaneous space measurements of
1066 atmospheric pollutants in the boundary layer from IASI: A case study in the North China Plain,
1067 *Geophys. Res. Lett.*, 41, 645–651, doi:10.1002/2013GL058333, 2014.
1068

1069 Brasseur, G. P. and D. J. Jacob, *Modeling of Atmospheric Chemistry*, Cambridge University Press,
1070 2017.
1071

1072 Brasseur, G. P., J. Orlando, and G. Tyndall, *Atmospheric Chemistry and Global Change*, Oxford
1073 University Press, New York, 1999.
1074

1075 Callies, J., Corpaccioli, E., Eisinger, M., Hahne, A., and Lefebvre, A.: GOME-2 – Metop’s Second
1076 Generation Sensor for Operational Ozone Monitoring, *ESA Bull.-Eur. Space*, 102, 28–36, 2000.
1077

1078 Chatani, S. and Sudo, K.: Influences of the variation in inflow to East Asia on surface ozone over Japan
1079 during 1996–2005, *Atmos. Chem. Phys.*, 11, 8745-8758, doi:10.5194/acp-11-8745-2011, 2011.
1080

1081 Chen, F., and J. Dudhia, Coupling an advanced land surface-hydrology model with the Penn State-
1082 NCAR MM5 modeling system. Part I: Model implementation and sensitivity. *Mon. Wea. Rev.*, 129,
1083 569-585, 2001.
1084

1085 Chin, M., P. Ginoux, S. Kinne, B. N. Holben, B. N. Duncan, R. V. Martin, J. A. Logan, A. Higurashi,
1086 and T. Nakajima, Tropospheric aerosol optical thickness from the GOCART model and comparisons
1087 with satellite and sunphotometer measurements, *J. Atmos. Sci.* 59, 461-483, 2002.
1088

1089 Chou, M., M.J. Suarez, C. Ho, M.M. Yan, and K. Lee, Parameterizations for Cloud Overlapping and
1090 Shortwave Single-Scattering Properties for Use in General Circulation and Cloud Ensemble Models. *J.*
1091 *Climate*, 11, 202–214, 1998.
1092

1093 Deeter, M. N., S. Martínez-Alonso, D. P. Edwards, L. K. Emmons, J. C. Gille, H. M. Worden, C.
1094 Sweeney, J. V. Pittman, B. C. Daube, and S. C. Wofsy, The MOPITT Version 6 product: algorithm
1095 enhancements and validation, *Atmos. Meas. Tech.*, 7(11), 3623–3632, doi:10.5194/amt-7-3623-2014,
1096 2014.

1097

1098 Emmons, L. K., Walters, S., Hess, P. G., Lamarque, J.-F., Pfister, G. G., Fillmore, D., Granier, C.,
1099 Guenther, A., Kinnison, D., Laepple, T., Orlando, J., Tie, X., Tyndall, G., Wiedinmyer, C., Baughcum,
1100 S. L., and Kloster, S.: Description and evaluation of the Model for Ozone and Related chemical Tracers,
1101 version 4 (MOZART-4), *Geosci. Model Dev.*, 3, 43-67, doi:10.5194/gmd-3-43-2010, 2010.

1102

1103 Eskes, H. J. and Boersma, K. F.: Averaging kernels for DOAS total-column satellite retrievals, *Atmos.*
1104 *Chem. Phys.*, 3, 1285-1291, doi:10.5194/acp-3-1285-2003, 2003.

1105

1106 Eskes, H., Huijnen, V., Arola, A., Benedictow, A., Blechschmidt, A.-M., Botek, E., Boucher, O.,
1107 Bouarar, I., Chabrillat, S., Cuevas, E., Engelen, R., Flentje, H., Gaudel, A., Griesfeller, J., Jones, L.,
1108 Kapsomenakis, J., Katragkou, E., Kinne, S., Langerock, B., Razinger, M., Richter, A., Schultz, M.,
1109 Schulz, M., Sudarchikova, N., Thouret, V., Vrekoussis, M., Wagner, A., and Zerefos, C.: Validation of
1110 reactive gases and aerosols in the MACC global analysis and forecast system, *Geosci. Model Dev.*, 8,
1111 3523-3543, <https://doi.org/10.5194/gmd-8-3523-2015>, 2015.

1112

1113 Fan, Q., Lan, J., Liu, Y., Wang, X., Chan, P., Hong, Y., Feng, Y., Liu, Y., Zeng, Y., Liang, G., Process
1114 analysis of regional aerosol pollution during spring in the Pearl River Delta region, China, *Atmos. Env.*,
1115 122, 829-838, 2015.

1116

1117 Fast, J. D., Gustafson Jr., W. I., Easter, R. C., Zaveri, R. A., Barnard, J. C., Chapman, E. G., Grell, G.
1118 A., and Peckham, S. E.: Evolution of ozone, particulates, and aerosol direct radiative forcing on the
1119 vicinity of Houston using a fully coupled meteorology-chemistry-aerosol model, *J. Geophys. Res.*,
1120 111,D21305, doi:10.1029/2005JD006721, 2006.

1121

1122 Flemming, J., Inness, A., Flentje, H., Huijnen, V., Moinat, P., Schultz, M. G., and Stein, O.: Coupling
1123 global chemistry transport models to ECMWF's integrated forecast system, *Geosci. Model Dev.*, 2,
1124 253–265, doi:10.5194/gmd-2-253-2009, 2009.

1125

1126 Flemming, J., Huijnen, V., Arteta, J., Bechtold, P., Beljaars, A., Blechschmidt, A.-M., Diamantakis, M.,
1127 Engelen, R. J., Gaudel, A., Inness, A., Jones, L., Josse, B., Katragkou, E., Marecal, V., Peuch, V.-H.,
1128 Richter, A., Schultz, M. G., Stein, O., and Tsikerdekis, A.: Tropospheric chemistry in the Integrated
1129 Forecasting System of ECMWF, *Geosci. Model Dev.*, 8, 975-1003, [https://doi.org/10.5194/gmd-8-975-](https://doi.org/10.5194/gmd-8-975-2015)
1130 2015, 2015.

1131

1132 Flemming, J., Benedetti, A., Inness, A., Engelen, R. J., Jones, L., Huijnen, V., Remy, S., Parrington, M.,
1133 Suttie, M., Bozzo, A., Peuch, V.-H., Akritidis, D., and Katragkou, E.: The CAMS interim Reanalysis of
1134 Carbon Monoxide, Ozone and Aerosol for 2003–2015, *Atmos. Chem. Phys.*, 17, 1945-1983,
1135 doi:10.5194/acp-17-1945-2017, 2017.

1136 Freitas, S. R., Longo, K. M., Chatfield, R., Latham, D., Silva Dias, M. A. F., Andreae, M. O., Prins, E.,
1137 Santos, J. C., Gielow, R., and Carvalho Jr., J. A.: Including the sub-grid scale plume rise of vegetation
1138 fires in low resolution atmospheric transport models, *Atmos. Chem. Phys.*, 7, 3385-3398,
1139 doi:10.5194/acp-7-3385-2007, 2007.

1140

1141 Fu, J. S., Hsu, N. C., Gao, Y., Huang, K., Li, C., Lin, N.-H., and Tsay, S.-C.: Evaluating the influences
1142 of biomass burning during 2006 BASE-ASIA: a regional chemical transport modeling, *Atmos. Chem.*
1143 *Phys.*, 12, 3837-3855, <https://doi.org/10.5194/acp-12-3837-2012>, 2012.

1144

1145 Geng, H., Hwang, H., Liu, X., Dong, S., and Ro, C.-U.: Investigation of aged aerosols in size-resolved
1146 Asian dust storm particles transported from Beijing, China, to Incheon, Korea, using low-Z particle
1147 EPMA, *Atmos. Chem. Phys.*, 14, 3307-3323, doi:10.5194/acp-14-3307-2014, 2014.

1148

1149 Ginoux, P., Chin, M., Tegen, I., Prospero, J. M., Holben, B., Dubovik, O., and Lin, S. J.: Sources and
1150 distributions of dust aerosols simulated with the GOCART model, *J. Geophys. Res. Atmos.*, 106,
1151 20255–20273, 2001.

1152

1153 Granier, C., B. Bessagnet, T. Bond, A. D'Angiola, H. Denier van der Gon, G.J. Frost, A. Heil, M.
1154 Kainuma, J. Kaiser, S. Kinne, Z. Klimont, S. Kloster, J.-F. Lamarque, C. Lioussé, T. Matsui, F. Meleux,
1155 A. Mieville, T. Ohara, K. Raihi, M. Schultz, S. J. Smith, A. M. Thomson, J. van Aardenne, and G.
1156 van der Werf, 2011, Evolution of anthropogenic and biomass burning emissions of air pollutants
1157 at global and regional scales during the 1980–2010 period, *Climatic Change*, 109:163- 190. DOI:
1158 10.1007/s10584-011-0154-1, 2011.

1159

1160 Granier, C., Doumbia, T., Granier, L., Sindelarova, K., Frost, G. J., Bouarar, I., Lioussé, C., Darras, S.
1161 and J. Stavrou, Anthropogenic Emissions in Asia. In: Bouarar I., Wang X. and Brasseur G.-P. (Eds.)
1162 *Air Pollution in Asia: An Integrated Perspective*. Springer, ISBN 978-3-319-59489-7, 2017.

1163

1164 Grell, G.A., S.E. Peckham, R. Schmitz, S.A. McKeen, G. Frost, W.C. Skamarock, B. Eder, Fully
1165 coupled online chemistry within the WRF model, *Atmos. Environ.*, 39, pp. 6957–6975, 2005.

1166

1167 Grell, G. A. and Freitas, S. R.: A scale and aerosol aware stochastic convective parameterization for
1168 weather and air quality modeling, *Atmos. Chem. Phys.*, 14, 5233-5250, doi:10.5194/acp-14-5233-2014,
1169 2014.

1170

1171 Guenther, A., Karl, T., Harley, P., Wiedinmyer, C., Palmer, P. I., and Geron, C.: Estimates of global
1172 terrestrial isoprene emissions using MEGAN (Model of Emissions of Gases and Aerosols from Nature),
1173 *Atmos. Chem. Phys.*, 6, 3181-3210, doi:10.5194/acp-6-3181-2006, 2006.

1174

1175 Guo, S., Hu, M., Zamora, M. L., Peng, J., Shang, D., Zheng, J., Du, Z., Wu, Z., Shao, M., Zeng, L.,
1176 Molina, M. J. and R. Zhang, Elucidating severe urban haze formation in China, *Proc. Natl. Acad. Sci.*
1177 *USA*, 111(49): 17373–17378., 2014.

1178 Hamra, G. B., Laden, F., Cohen, A. J., Raaschou-Nielsen, O., Brauer, M., and D. Loomis, Lung Cancer
1179 and Exposure to Nitrogen Dioxide and Traffic: A Systematic Review and Meta-Analysis, *Environ*
1180 *Health Perspect*, 123 | 11, DOI:10.1289/ehp.1408882, 2015.

1181 Hong, S. Y., Y. Noh, and J. Dudhia, A new vertical diffusion package with an explicit treatment of
1182 entrainment processes, *Mon. Weather Rev.*, 134(9), 2318–2341, doi:10.1175/Mwr3199.1, 2006.

1183
1184 Huang, K., Zhuang, G., Wang, Q., Fu, J. S., Lin, Y., Liu, T., Han, L., and Deng, C.: Extreme haze
1185 pollution in Beijing during January 2013: chemical characteristics, formation mechanism and role of
1186 fog processing, *Atmos. Chem. Phys. Discuss.*, 14, 7517-7556, doi:10.5194/acpd-14-7517-2014, 2014.

1187
1188 Huang, R.-J., Y. Zhang, et al., High secondary aerosol contribution to particulate pollution during haze
1189 events in China. *Nature* 514(7521): 218-222, 2014.

1190
1191 Inness, A., Baier, F., Benedetti, A., Bouarar, I., Chabrillat, S., Clark, H., Clerbaux, C., Coheur, P.,
1192 Engelen, R. J., Errera, Q., Flemming, J., George, M., Granier, C., Hadji-Lazarou, J., Huijnen, V.,
1193 Hurtmans, D., Jones, L., Kaiser, J. W., Kapsomenakis, J., Lefever, K., Leitão, J., Razinger, M., Richter,
1194 A., Schultz, M. G., Simmons, A. J., Suttie, M., Stein, O., Thépaut, J.-N., Thouret, V., Vrekoussis, M.,
1195 Zerefos, C., and the MACC team: The MACC reanalysis: an 8 yr data set of atmospheric composition,
1196 *Atmos. Chem. Phys.*, 13, 4073–4109, doi:10.5194/acp-13-4073-2013, 2013.

1197
1198 Jacob, D. J., J. A. Logan, and P. P. Murti, Effect of rising Asian emissions on surface ozone in the
1199 United States, *Geophys. Res. Lett.*, 26, 2175–2178, 1999.

1200
1201 Janssens-Maenhout, G., Crippa, M., Guizzardi, D., Dentener, F., Muntean, M., Pouliot, G., Keating, T.,
1202 Zhang, Q., Kurokawa, J., Wankmüller, R., Denier van der Gon, H., Kuenen, J. J. P., Klimont, Z., Frost,
1203 G., Darras, S., Koffi, B., and Li, M.: HTAP_v2.2: a mosaic of regional and global emission grid maps
1204 for 2008 and 2010 to study hemispheric transport of air pollution, *Atmos. Chem. Phys.*, 15, 11411-
1205 11432, doi:10.5194/acp-15-11411-2015, 2015.

1206
1207 Jiménez, P. A., and J. Dudhia, Improving the Representation of Resolved and Unresolved Topographic
1208 Effects on Surface Wind in the WRF Model. *J. Appl. Meteor. Climatol.*, 51, 300–316, doi:
1209 10.1175/JAMC-D-11-084.1, 2012.

1210
1211 Kurokawa, J., Ohara, T., Uno, I., Hayasaki, M., and Tanimoto, H.: Influence of meteorological
1212 variability on interannual variations of springtime boundary layer ozone over Japan during 1981–2005,
1213 *Atmos. Chem. Phys.*, 9, 6287-6304, doi:10.5194/acp-9-6287-2009, 2009.

1214
1215 Kurokawa, J., Ohara, T., Morikawa, T., Hanayama, S., Janssens-Maenhout, G., Fukui, T., Kawashima,
1216 K., and Akimoto, H.: Emissions of air pollutants and greenhouse gases over Asian regions during 2000–
1217 2008: Regional Emission inventory in ASia (REAS) version 2, *Atmos. Chem. Phys.*, 13, 11019-11058,
1218 doi:10.5194/acp-13-11019-2013, 2013.

1219
1220 Kampa, M., and Castanas, E., Human health effects of air pollution, *Environmental Pollution*, 151:362–
1221 367, DOI: 10.1016/j.envpol.2007.06.012, 2008.

1222
1223 Kang et al., New Categorical Metrics for Air Quality Model Evaluation, *J. Appl. Meteorol. Climatol.*,
1224 2006.
1225
1226 Leisner, C. P. and Ainsworth, E. A.: Quantifying the effects of ozone on plant reproductive growth and
1227 development, *Global Change Biol.*, 18, 606–616, 2012.
1228
1229 Liang, Q., Jaeglé, L., Jaffe, D. A., Weiss-Penzias, P., Heckman, A., and Snow, J. A.: Long-range
1230 transport of Asian pollution to the northeast Pacific: Seasonal variations and transport pathways of
1231 carbon monoxide, *J. Geophys. Res.*, 109, D23S07, doi:10.1029/2003JD004402, 2004.
1232
1233 Liao, J., Wang, T., Wang, X., Xie, M., Jiang, Z., Huang, X., Zhu, J., Impacts of different urban canopy
1234 schemes in WRF/Chem on regional climate and air quality in Yangtze_River_Delta, China, *J. Atmos.*
1235 *Res.*, 145–146:226-243, DOI: 10.1016/j.atmosres.2014.04.005, 2014.
1236
1237 Lin, M., Fiore, A. M., Horowitz, L.W., Cooper, O. R., Naik, V., Holloway, J., Johnson, B. J.,
1238 Middlebrook, A. M., Oltmans, S. J., Pollack, I. B., Ryerson, T. B., Warner, J. X. and Wiedinmyer, C.,
1239 and Wilson, J., Wyman, B., Transport of Asian ozone pollution into surface air over the western United
1240 States in spring, *J. Geophys. Res.*, 117(D21), 2156-2202, doi:10.1029/2011JD016961, 2012.
1241
1242 Ma, J., Richter, A., Burrows, J.P., Nüß, H., VanAardenne, J.A., Comparison of model-simulated
1243 tropospheric NO₂ over China with GOME-satellite data. *Atmospheric Environment*, 40 . pp. 593-604,
1244 2006.
1245
1246 Marécal, V., Peuch, V.-H., Andersson, C., Andersson, S., Arteta, J., Beekmann, M., Benedictow, A.,
1247 Bergström, R., Bessagnet, B., Cansado, A., Chéroux, F., Colette, A., Coman, A., Curier, R. L., Denier
1248 van der Gon, H. A. C., Drouin, A., Elbern, H., Emili, E., Engelen, R. J., Eskes, H. J., Foret, G., Friese,
1249 E., Gauss, M., Giannaros, C., Guth, J., Joly, M., Jaumouillé, E., Josse, B., Kadygrov, N., Kaiser, J. W.,
1250 Krajsek, K., Kuenen, J., Kumar, U., Liora, N., Lopez, E., Malherbe, L., Martinez, I., Melas, D., Meleux,
1251 F., Menut, L., Moinat, P., Morales, T., Parmentier, J., Piacentini, A., Plu, M., Poupkou, A., Queguiner,
1252 S., Robertson, L., Rouil, L., Schaap, M., Segers, A., Sofiev, M., Tarasson, L., Thomas, M.,
1253 Timmermans, R., Valdebenito, Á., van Velthoven, P., van Versendaal, R., Vira, J., and Ung, A.: A
1254 regional air quality forecasting system over Europe: the MACC-II daily ensemble production, *Geosci.*
1255 *Model Dev.*, 8, 2777-2813, <https://doi.org/10.5194/gmd-8-2777-2015>, 2015.
1256
1257 Martin, R. V., Chance, K., Jacob, D. J., et al.: An Improved Retrieval of Tropospheric Nitrogen Dioxide
1258 from GOME, *J. Geophys. Res.*, 107 (D20), 4437–4457, doi:10.1029/2001JD001027, 2002.
1259
1260 Mlawer, E. J., S. J. Taubman, P. D. Brown, M. J. Iacono, and S. A. Clough, Radiative transfer for
1261 inhomogeneous atmosphere: RRTM, a validated correlated-k model for the longwave. *J. Geophys. Res.*,
1262 102(D14), 16 663–16 682, 1997.
1263
1264 Osada, K., Ohara, T., Uno, I., Kido, M., and Iida, H.: Impact of Chinese anthropogenic emissions on
1265 submicrometer aerosol concentration at Mt. Tateyama, Japan, *Atmos. Chem. Phys.*, 9, 9111-9120,
1266 doi:10.5194/acp-9-9111-2009, 2009.

1267
1268 Quennehen, B., Raut, J.-C., Law, K. S., Daskalakis, N., Ancellet, G., Clerbaux, C., Kim, S.-W., Lund,
1269 M. T., Myhre, G., Oliv  , D. J. L., Safieddine, S., Skeie, R. B., Thomas, J. L., Tsyro, S., Bazureau, A.,
1270 Bellouin, N., Hu, M., Kanakidou, M., Klimont, Z., Kupiainen, K., Myriokefalitakis, S., Quaas, J.,
1271 Rumbold, S. T., Schulz, M., Cherian, R., Shimizu, A., Wang, J., Yoon, S.-C., and Zhu, T.: Multi-model
1272 evaluation of short-lived pollutant distributions over east Asia during summer 2008, *Atmos. Chem.*
1273 *Phys.*, 16, 10765-10792, doi:10.5194/acp-16-10765-2016, 2016.

1274
1275 Richter, A., and J. P. Burrows, Tropospheric NO₂ from GOME measurements, *Adv. Space Res.*, 29,
1276 1673–1683, 2002.

1277
1278 Sinha, B., Singh Sangwan, K., Maurya, Y., Kumar, V., Sarkar, C., Chandra, B. P., and Sinha, V.:
1279 Assessment of crop yield losses in Punjab and Haryana using 2 years of continuous in situ ozone
1280 measurements, *Atmos. Chem. Phys.*, 15, 9555-9576, doi:10.5194/acp-15-9555-2015, 2015.

1281
1282 Sitch, S., Cox, P.M., Collins, W.J., Huntingford, C., Indirect radiative forcing of climate change through
1283 ozone effects on the land-carbon sink. *Nature*. 448: 791-794, 2007.

1284
1285 Skamarock, W. C., and Coauthors, A description of the Advanced Research WRF version 3. NCAR
1286 Tech. Note NCAR/TN-4751 STR, 125 pp. [http://www2.mmm.ucar.edu/wrf/users/docs/arw_v3.pdf],
1287 2008.

1288 Stein, O., Schultz, M. G., Bouarar, I., Clark, H., Huijnen, V., Gaudel, A., George, M., and Clerbaux, C.:
1289 On the wintertime low bias of Northern Hemisphere carbon monoxide found in global model
1290 simulations, *Atmos. Chem. Phys.*, 14, 9295-9316, <https://doi.org/10.5194/acp-14-9295-2014>, 2014.

1291
1292 Stohl, A., Forster, C., Huntrieser, H., Mannstein, H., McMillan, W. W., Petzold, A., Schlager, H., and
1293 Weinzierl, B.: Aircraft measurements over Europe of an air pollution plume from Southeast Asia –
1294 aerosol and chemical characterization, *Atmos. Chem. Phys.*, 7, 913-937, doi:10.5194/acp-7-913-2007,
1295 2007.

1296
1297 Thompson, G., Rasmussen, R. M., and K. Manning, Explicit forecasts of winter precipitation using an
1298 improved bulk microphysics scheme. Part I: Description and sensitivity analysis. *Mon. Wea. Rev.*, 132,
1299 519–542, 2004.

1300
1301 Thompson, G., Field, P. R., Rasmussen, R. M., and W. D. Hall, Explicit forecasts of winter
1302 precipitation using an improved bulk microphysics scheme. Part II: Implementation of a new snow
1303 parameterization. *Mon. Wea. Rev.*, 136, 5095–5115, 2008.

1304
1305 Tuccella, P., Curci, G., Visconti, G., Bessagnet, B., Menut, L., and Park, R. J.: Modeling of gas and
1306 aerosol with WRF/Chem over Europe: Evaluation and sensitivity study, *J. Geophys. Res.-Atmos.*, 117,
1307 D03303, doi:10.1029/2011jd016302, 2012.

1308
1309 UNECE, 2010. Hemispheric Transport of Air Pollution 2010: Part A, Ozone and Particulate Matter. Air
1310 Pollution Studies N0 17. Dentener, F., Keating, T., and Akimoto, H. (Eds.), United Nations Publication,
1311 New York and Geneva (2010) ECE/EB.AIR/100.

1312
1313 Wagner, A., Blechschmidt, A.-M., Bouarar, I., Brunke, E.-G., Clerbaux, C., Cupeiro, M., Cristofanelli,
1314 P., Eskes, H., Flemming, J., Flentje, H., George, M., Gilge, S., Hilboll, A., Inness, A., Kapsomenakis,
1315 J., Richter, A., Ries, L., Spangl, W., Stein, O., Weller, R., and Zerefos, C.: Evaluation of the MACC
1316 operational forecast system – potential and challenges of global near-real-time modelling with respect to
1317 reactive gases in the troposphere, *Atmos. Chem. Phys.*, 15, 14005-14030, doi:10.5194/acp-15-14005-
1318 2015, 2015.

1319
1320 Wang, X., and Coauthors, WRF-Chem simulation of East Asian air quality: Sensitivity to temporal and
1321 vertical emissions distributions. *Atmos. Environ.*, 44, 660–669, doi:10.1016/J. Atmos. Env.
1322 2009.11.011, 2010.

1323
1324 Wang, Y., Yao, L., Wang, L., Ji, D., Tang, G., Zhang, J., Sun, Y., Hu, B., Xin, J., Mechanism for the
1325 formation of the January 2013 heavy haze pollution episode over central and eastern China, *Sci. China
1326 Earth Sci.*, 57: 14. doi:10.1007/s11430-013-4773-4, 2014.

1327
1328 Wiedinmyer, C., Akagi, S. K., Yokelson, R. J., Emmons, L. K., Al-Saadi, J. A., Orlando, J. J., and Soja,
1329 A. J.: The Fire INventory from NCAR (FINN): a high resolution global model to estimate the emissions
1330 from open burning, *Geosci. Model Dev.*, 4, 625-641, doi:10.5194/gmd-4-625-2011, 2011.

1331
1332 Willmott, C.J., Robeson, S.M., Matsuura, K., A refined index of model performance. *International
1333 Journal of Climatology* 32, 2088-2094. <http://dx.doi.org/10.1002/joc.2419>, 2012.

1334
1335 Wilks, D.S., *Statistical Methods in the Atmospheric Sciences*, 2nd Edition, Elsevier, New York, 2006.

1336
1337 Wu, Q., Wang, Z., Chen, H., Zhou, W., Wenig, M., An evaluation of air quality modeling over the Pearl
1338 River Delta during November 2006, *Meteorol. Atmos. Phys.*, 116: 113. doi:10.1007/s00703-011-0179-
1339 z, 2012.

1340
1341 Zaveri, R. A., Easter, R. C., Fast, J. D., Peters, L. K., Model for Simulating Aerosol Interactions and
1342 Chemistry (MOSAIC), *J. Geophys. Res.*, 113, D13204, doi:10.1029/2007JD008782, 2008.

1343
1344 Zhao, X. J., Zhao, P. S., Xu, J., Meng,, W., Pu, W. W., Dong, F., He, D., and Shi, Q. F.: Analysis of a
1345 winter regional haze event and its formation mechanism in the North China Plain, *Atmos. Chem. Phys.*,
1346 13, 5685-5696, doi:10.5194/acp-13-5685-2013, 2013.

1347
1348 Zhang, L., Jacob, *D. J.*, Kopacz, *M.*, Henze, *D. K.*, Singh, *K.*, and Jaffe, *D. A.*, Intercontinental source
1349 attribution of ozone pollution at western U.S. sites using an adjoint method, *Geophys. Res. Lett.*, 36,
1350 *L11810*, doi:10.1029/2009GL037950, 2009.

1351
1352 Zhang, Y., Wen, X.-Y., and Jang, C., Simulating chemistry–aerosol–cloud–radiation–climate feedbacks
1353 over the continental US using the online-coupled Weather Research Forecasting Model with chemistry
1354 (WRF/Chem), *Atmos. Environ.*, 44, 3568–3582, 2010.

1355

- 1356 Zhang, B., Wang, Y., and Hao, J., Simulating aerosol–radiation–cloud feedbacks on meteorology and
1357 air quality over eastern China under severe haze conditions in winter, *Atmos. Chem. Phys.*, 15, 2387-
1358 2404, doi:10.5194/acp-15-2387-2015, 2015.
- 1359
- 1360 Xu, J., Zhang, Y., Fu, J.S., Zheng, S., Wang, W., Process analysis of typical summertime ozone
1361 episodes over the Beijing area, *Science of The Total Environment*, Volume 399, Issues 1–3, 25 July
1362 2008, Pages 147-157, ISSN 0048-9697, <http://dx.doi.org/10.1016/j.scitotenv.2008.02.013>, 2008.